

# The anomalous and smoothed anomalous envelope spectra for rotating machine fault diagnosis

Stephan Schmidt<sup>a,\*</sup>, Konstantinos C. Gryllias<sup>b,c</sup>

<sup>a</sup>*Centre for Asset Integrity Management, Department of Mechanical and Aeronautical Engineering, University of Pretoria, Pretoria, South Africa*

<sup>b</sup>*Department of Mechanical Engineering, KU Leuven, Celestijnenlaan 300, 3001 Heverlee, Belgium*

<sup>c</sup>*Dynamics of Mechanical and Mechatronic Systems, Flanders Make, Belgium*

---

## Abstract

The order-frequency spectral coherence and its integrated spectra (e.g. improved envelope spectrum, squared envelope spectrum) are some of the most powerful methods for performing fault diagnosis under time-varying operating conditions. However, it may require much work to interrogate the order-frequency spectral coherence for symptoms of damage. Hence, in this work we propose a methodology that combines the order-frequency spectral coherence with historical data that were acquired from a healthy machine to obtain an anomalous envelope spectrum, which is further processed for fault diagnosis. This anomalous envelope spectrum is further processed with a smoothing operation to not only perform automatic fault detection, but it is also possible to identify the damaged component if the kinematics of the gearbox are known. The proposed method is investigated on one numerical gearbox dataset and three experimental datasets, where its potential for performing automatic fault detection under time-varying operating conditions is highlighted.

*Keywords:*

Anomalous envelope spectrum, Cyclostationary analysis, Novelty detection, Blind fault detection, Time-varying operating conditions

---

\*Corresponding author.

*Email address:* `stephan.schmidt@up.ac.za` (Stephan Schmidt)

## 1. Introduction

The vibration signals acquired from rotating machines are usually generated by periodic phenomena (e.g. gear mesh interactions, impacts due to bearing damage) [1]. As a result, the statistics of the signal are periodic in the angle domain and therefore the measured vibration signals can be described by the theory of cyclostationarity [1, 2]. This makes cyclostationary analysis techniques such as the squared envelope spectrum [3, 4], the instantaneous power spectrum [5, 6], the spectral correlation [7, 8] and the spectral coherence [7, 8] very powerful techniques for interrogating the vibration signals for symptoms of damage.

However, rotating machines such as wind turbines operate inherently under time-varying operating conditions [5, 9], which impedes the application of the conventional time- or angle-based cyclostationary techniques [10]. This is attributed to the fact that even though the instantaneous power of the bearing damage component is periodic in the angle domain, the carrier of the signal is described by the dynamic properties of the structure, which are time-invariant [10]. Hence, neither the time nor angle domain representations are suited to describe these signals, and the signals should rather be described using angle-time cyclostationary theory [10]. Hence, the angle-frequency instantaneous power spectrum [5], the order-frequency spectral correlation [10] and Order-Frequency Spectral Coherence (OFSCoh) [10] should be used for analysing the time-invariant second-order components of vibration signals that were acquired under time-varying speed conditions.

The OFSCoh is currently one of the most powerful techniques for performing bearing diagnostics under time-varying operating conditions [10]. It is a bivariate representation of the cyclic orders of the angle-periodic modulation components and the spectral frequencies of their time-invariant carriers [10]. However, the two-dimensional representation can be difficult to interrogate when incipient damage is present and therefore the integrated spectral coherence is very useful for fault diagnosis [8, 11–13].

However, applying state-of-the-art signal analysis techniques can require much work to implement and much manual effort to investigate for symptoms of damage. In some

1  
2  
3 cases the fault order of the component-of-interest needs to be specified a priori before  
4 the method can be applied e.g., [2, 12, 14]. This means that the techniques could be  
5 difficult to scale when many machines need to be monitored for damage. This has been  
6 one of the main motivations of developing deep learning fault diagnosis methods [15]; the  
7 methods make it possible to automatically determine the condition of the machine from  
8 the raw or processed vibration signals. Chen et al. [16] combined the spectral coherence  
9 and convolutional neural networks for automatic fault classification. However, many deep  
10 learning methods require much historical fault data to be available and the classification  
11 problem is actually an open set recognition problem (i.e. only historical fault data of  
12 some of the damage modes may be available), which could make it difficult to apply the  
13 supervised learning techniques in practice [17].

14  
15  
16 In Ref. [14], a methodology is proposed to combine the OFSCoh with healthy histor-  
17 ical data. This is performed by firstly identifying the damage modes in the system and  
18 targeting their specific cyclic orders in the OFSCoh. Subsequently, a data-driven model  
19 was developed of the healthy behaviour of the features extracted from the targeted compo-  
20 nents, which was then used to automatically infer the health of the targeted components.  
21 However, if a complex drive train is under consideration, there may be many cyclic orders  
22 that need to be targeted to properly monitor the machine. It is also possible that the  
23 harmonics of the cyclic orders of different components can overlap, which may lead to  
24 ambiguous behaviour when performing inference.

25  
26 Hence, in this work we propose a blind methodology that can be used for performing  
27 fault diagnosis under time-varying operating conditions. The outcome of this methodology  
28 is the Anomalous Envelope Spectrum (AES) and the smoothed AES (sAES), which are  
29 calculated by combining the OFSCoh and historical data from a healthy machine. The  
30 AES is a powerful representation that can be used to detect faults and it can also help  
31 to identify which components are damaged. It has the additional benefit, compared to  
32 Ref. [14] for example, that it does not require the components-of-interest to be known  
33 nor specified before applying the methodology, i.e. it is blind. It is only desirable to know  
34  
35  
36  
37  
38  
39  
40  
41  
42  
43  
44  
45  
46  
47  
48  
49  
50  
51  
52  
53  
54  
55  
56  
57  
58  
59  
60  
61  
62  
63  
64  
65

1  
2  
3 the kinematics of the gearbox if the AES is interrogated to determine which machine  
4  
5 component is damaged.  
6

7 In summary, the contributions of this paper are the following:  
8

- 9
- 10 • A new representation, the Anomalous Envelope Spectrum (AES), is proposed which  
11 can be processed to perform fault diagnosis under time-varying operating conditions.  
12 We propose using a smoothing operation between consecutive OFSCohs before the  
13 AES is calculated. This processed AES is referred to as the smoothed AES (sAES)  
14 in this work.  
15
  - 16 • This method is simple to implement and scalable for monitoring many machines.  
17 This is because historical data are used to supplement the OFSCoh for fault detection  
18 and identification under time-varying operating conditions, i.e. it is not necessary  
19 to manually interrogate the signals.  
20

21 The layout of the paper is as follows: In Section 2, an overview of the proposed  
22 method is given, whereafter the method is applied on numerical gearbox data in Section  
23 3 and on three experimental gearbox datasets in Section 4. In Section 5, additional  
24 analyses are performed to quantify the calculation time of the proposed method and to  
25 highlight the influence of the historical data on the proposed method. Finally, the paper  
26 is concluded in Section 6. Appendix A contains additional information pertaining to the  
27 threshold selection discussed in Section 2; Appendix B contains additional information of  
28 the numerical gearbox model presented in Section 3; and Appendix C contains additional  
29 results obtained on the experimental data discussed in Section 4.  
30

## 31 **2. Proposed methodology**

32

33 We desire to develop a vibration-based condition monitoring methodology that enables  
34 us to determine the condition of the machine at measurement  $i$ , without requiring the  
35 cyclic orders of interest to be specified beforehand, i.e. the methodology is blind. This  
36 methodology is developed under the following assumptions:  
37  
38  
39  
40  
41  
42  
43  
44  
45  
46  
47  
48  
49  
50  
51  
52  
53  
54  
55  
56  
57  
58  
59  
60  
61  
62  
63  
64  
65

- There are much historical data available that describe the behaviour of the machine in a reference condition, whereafter the machine is monitored for damage.
- An accurate estimate of the rotational speed is available at each measurement, with the rotational speed at measurement  $i$  denoted by  $\omega^{(i)}(t)$ . If the speed cannot be measured, it is possible to use a tachless speed estimation method [18, 19] before applying this methodology.
- Regular measurements are taken during the condition monitoring process. The vibration signal acquired at measurement  $i$  is denoted by  $x^{(i)}(t)$  and its corresponding sampling frequency is  $f_s$ .

### 2.1. Preliminary theory

The Order-Frequency Spectral Coherence (OFSCoh) can highlight weak damage components in the signal and therefore enables incipient damage to be detected [10, 11]. The OFSCoh of the vibration measurement acquired at time step  $i$  [10]

$$\gamma^{(i)}(\alpha, f) = \frac{S_{xx}^{(i)}(\alpha, f)}{\left| S_x^{(i)}(0, f) \cdot S_{x_\alpha}^{(i)}(0, f) \right|^{1/2}}, \quad (1)$$

is calculated with the order-frequency spectral correlation  $S_{xx}^{(i)}(\alpha, f)$ , the power spectral density of the vibration signal  $x^{(i)}(t)$  denoted by  $S_x^{(i)}(0, f)$  and the power spectral density of  $x_\alpha^{(i)}(t) = x^{(i)}(t) \cdot e^{-j\alpha\theta^{(i)}(t)} \cdot \omega^{(i)}(t)$  denoted by  $S_{x_\alpha}^{(i)}(0, f)$  [10]. The imaginary unit is denoted by  $j = \sqrt{-1}$ . In Equation (1),  $\alpha$  denotes the cyclic order variable and  $f$  denotes the spectral frequency variable. The order-frequency spectral correlation is calculated with [10]

$$S_{xx}^{(i)}(\alpha, f) = \lim_{W \rightarrow \infty} \frac{1}{\Phi(W)} \mathbb{E} \left\{ \mathcal{F}_W(x^{(i)}(t))^* \cdot \mathcal{F}_W \left( x^{(i)}(t) \cdot e^{-j\alpha\theta^{(i)}(t)} \cdot \omega^{(i)}(t) \right) \right\}, \quad (2)$$

where  $\mathcal{F}_W(\cdot)$  is the Fourier transform over a time length of  $W$ ,  $x^{(i)}(t)$  is the measurement taken at time step  $i$ ,  $\omega^{(i)}(t)$  is the corresponding instantaneous rotational speed of a shaft

1  
2  
3 and  $\theta^{(i)}(t)$  is the corresponding instantaneous phase of the shaft. The cumulative phase of  
4  
5 the shaft after a time duration of  $W$  is denoted  $\Phi(W)$ . The reason why the measurement  
6  
7 index  $i$  is emphasised in all of the terms, is because this is important for the calculation of  
8  
9 the processed AES and it ensures that a consistent notation is used. The order-frequency  
10  
11 spectral correlation is estimated with the Welch-based estimator proposed in Ref. [10], due  
12  
13 to its good bias and variance properties. However, much faster estimators of the spectral  
14  
15 correlation can be used if desired [11, 20].

16  
17 The integrated spectral coherence is very useful for gearbox diagnostics, due to the  
18  
19 fact that it is simpler to interrogate for damage than the bivariate OFSCoh [12, 13]. The  
20  
21 Squared Envelope Spectrum is the most popular signal analysis technique for performing  
22  
23 bearing fault diagnosis [4] and can be estimated from the OFSCoh with [11, 13, 21]

$$24 \quad \text{SES}^{(i)}(\alpha) = \left| \int_0^{f_s/2} \gamma^{(i)}(\alpha, f) df \right|, \quad (3)$$

25  
26  
27 for the  $i$ th signal, while the enhanced envelope spectrum can be estimated with

$$28 \quad \text{EES}^{(i)}(\alpha) = \int_0^{f_s/2} |\gamma^{(i)}(\alpha, f)|^2 df. \quad (4)$$

29  
30  
31 The sampling frequency of the signal is denoted by  $f_s$ . It was shown in Ref. [11] that in  
32  
33 general the EES is better suited for incipient fault detection than the SES. Hence, it is  
34  
35 possible to estimate the SES and the EES with Equations (3) and (4) without performing  
36  
37 bandpass filtering on the raw vibration signal.

38  
39 It is possible to improve the signal-to-noise ratio of the damaged components in the  
40  
41 integrated spectrum by limiting the integration band of the SES and the EES to a band  
42  
43  $[f_l, f_h]$ . This is because the impulses generated by damaged components excite resonances  
44  
45 in the system, which means that the fault information manifests in narrow frequency bands  
46  
47 [22]. The integration of the OFSCoh over the band  $[f_l, f_h]$  is used to define the Improved  
48  
49  
50  
51  
52  
53  
54  
55  
56  
57  
58  
59  
60  
61  
62  
63  
64  
65

Envelope Spectrum (IES) [11],

$$\text{IES}^{(i)}(\alpha; f_l, f_h) = \int_{f_l}^{f_h} |\gamma^{(i)}(\alpha, f)|^2 df, \quad (5)$$

where  $0 < f_l < f_h$  and  $f_h < f_s/2$ . Therefore, if the integration band  $[f_l, f_h]$  is carefully selected, the IES can improve the signal-to-noise ratio of the fault information. However, selecting the appropriate frequency band automatically can be difficult to perform, especially if the fault information is weak. This has resulted in the development of the IESFOgram, which aims to detect the frequency band that is optimal for detecting specific targeted signal components [23]. Even though the IESFOgram performs very well in identifying the optimal integration band, it requires the targeted cyclic orders to be specified a priori. This can be difficult when complicated drive-trains with many fault orders need to be monitored or when the fault orders are not known.

The proposed methodology was developed to allow us to automatically identify the frequency bands that have important information and then to use this to obtain an intuitive representation for fault diagnosis. The Anomalous Envelope Spectrum (AES) is presented in the next section.

## 2.2. Anomalous Envelope Spectrum (AES)

The AES is derived from the Generalised Integrated Spectrum (GIS) in this work. The GIS of the  $i$ th vibration measurement is obtained from the integrated spectrum of the OFSCoh by including a general weighting function  $\mathcal{G}(\alpha, f)$

$$\text{GIS}^{(i)}(\alpha) = \int_0^{f_s/2} |\gamma^{(i)}(\alpha, f)|^2 \cdot \mathcal{G}(\alpha, f) df, \quad (6)$$

where the weighting function  $0 \leq \mathcal{G}(\alpha, f) \leq 1$ . This GIS has the following properties:

- The EES is obtained by setting  $\mathcal{G}(\alpha, f) = 1 \forall f \in [0, f_s/2]$ , i.e. then  $\text{GIS}^{(i)}(\alpha) = \text{EES}^{(i)}(\alpha)$ .

- The IES is obtained by setting  $\mathcal{G}(\alpha, f) = 1 \forall f \in [f_l, f_h]$  and  $\mathcal{G}(\alpha, f) = 0 \forall f \notin [f_l, f_h]$ , i.e. then  $\text{GIS}^{(i)}(\alpha) = \text{IES}^{(i)}(\alpha; f_l, f_h)$ .

Since it is assumed that healthy historical data are available, it is possible to construct a function  $G(\alpha, f)$  to automatically highlight regions in the OFSCoh that have non-healthy (i.e. anomalous) behaviour. This anomaly function  $G(\alpha, f)$  indicates whether healthy ( $G(\alpha, f) = 0$ ) or anomalous ( $G(\alpha, f) = 1$ ) behaviour is seen at a cyclic order  $\alpha$  and a spectral frequency  $f$  in  $|\gamma^{(i)}(\alpha, f)|^2$ . If we use this anomaly function  $G(\alpha, f)$  in the GIS, the Anomalous Envelope Spectrum (AES)

$$\text{AES}^{(i)}(\alpha) = \int_0^{f_s/2} |\gamma^{(i)}(\alpha, f)|^2 \cdot G(\alpha, f) df, \quad (7)$$

is obtained. The AES is used to identify components that are anomalous (e.g. attributed to machine damage or spurious noise). Hence, as opposed to selecting or estimating the optimal  $f_l$  and  $f_h$  to determine the IES with the GIS, only the information from anomalous frequency bands are retained in the AES.

### 2.3. Estimation of the AES

The OFSCohs associated with the  $N_h$  measurements from a healthy machine, denoted by  $\{\gamma_h^{(i)}(\alpha, f)\}_{i \in \mathbb{Z}, 0 \leq i \leq N_h - 1}$ , are used to calculate a threshold  $\tau(\alpha, f)$ . This threshold is used to automatically determine whether a specific combination of cyclic orders and spectral frequencies of the  $i$ th measurement contain anomalous information  $|\gamma^{(i)}(\alpha, f)|^2 > \tau(\alpha, f)$  or not  $|\gamma^{(i)}(\alpha, f)|^2 \leq \tau(\alpha, f)$ . This is used to define the anomaly function  $G$  for the measurement at time step  $i$  as follows:

$$G^{(i)}(\alpha, f) = \begin{cases} 1 & \text{if } |\gamma^{(i)}(\alpha, f)|^2 > \tau(\alpha, f) \\ 0 & \text{if } |\gamma^{(i)}(\alpha, f)|^2 \leq \tau(\alpha, f). \end{cases} \quad (8)$$

It is possible to use kernel density estimators to detect anomalous behaviour with the spectral coherence as investigated in Ref. [14], however, this can be computationally



intensive to use and it is required to find the optimal hyperparameters for each combination of  $\alpha$  and  $f$ . If it is assumed that the data are Gaussian, the threshold can be defined by:

$$\tau(\alpha, f) = \mu_\gamma(\alpha, f) + \kappa \cdot \sigma_\gamma(\alpha, f), \quad (9)$$

where  $\kappa$  is a factor,  $\mu_\gamma(\alpha, f)$  is the mean and  $\sigma_\gamma(\alpha, f)$  is the standard deviation of the healthy spectral coherences. However, the sampling distribution of the spectral coherence is not expected to be Gaussian. In Ref. [7], it was shown that the distribution of the spectral coherence is asymptotically chi-square distributed. Using the empirical distribution of the data to set the threshold is another approach that can be used. For example, the inter-percentile range can be used to obtain a threshold with

$$\tau(\alpha, f) = \kappa \cdot (p_\xi(\alpha, f) - p_{100-\xi}(\alpha, f)) + p_{100-\xi}(\alpha, f), \quad (10)$$

where  $p_\xi(\alpha, f)$  is the  $\xi$ th percentile of the set of healthy spectral coherences, denoted by  $\{\gamma_h^{(i)}(\alpha, f)\}$ , at a specific cyclic order  $\alpha$  and spectral frequency  $f$ . A special case of this range is the interquartile range where  $\xi = 75$ . If  $\kappa = 1$ , it means that the  $\xi$ th percentile is used for detecting outliers, which could result in false alarms. In addition to this, the threshold in Equation (10) is estimated from limited healthy measurements and is therefore a random variable. Hence, it is therefore suggested that  $\kappa > 1$ . In a practical situation, it would be better to use different  $\kappa$ s to obtain a range of thresholds for decision making, e.g. one threshold can act as a warning and another threshold can automatically stop the machine. The interpretation and use of the threshold would depend on the machine and its application (e.g. implications of a sudden failure).

The OFSCoh is estimated from a finite length signal and since the OFSCoh is sensitive to weak components in the signal, it could contain spurious noise. This would result in the anomaly function  $G^{(i)}(\alpha, f)$  to indicate anomalous behaviour, i.e.  $G^{(i)}(\alpha, f) = 1$ , for healthy cyclic orders and spectral frequencies. The robustness of the AES can be increased

by utilising the information from consecutive measurements to obtain the smoothed AES (sAES), which is a more robust representation of the condition of the gearbox under consideration. The smoothed AES (sAES) is calculated with

$$\text{sAES}^{(i)}(\alpha) = \int_0^{f_s/2} \mathcal{P} \{ |\gamma^{(m)}(\alpha, f)|^2 \cdot G^{(m)}(\alpha, f) \}_{m \in \mathbb{Z}, i - N_s \leq m \leq i} df, \quad (11)$$

where  $N_s$  is the number of consecutive measurements that is used for processing the weighted spectral coherences  $|\gamma^{(m)}(\alpha, f)|^2 \cdot G^{(m)}(\alpha, f)$ . We refer to this AES as the smoothed AES so that it is not confused with the raw AES obtained with Equation (7). The smoothing function  $\mathcal{P}$  can for example be the median or the mean. If the mean is used, the integrated spectrum of the moving averaged OFSCoh, i.e. the average of  $|\gamma^{(m)}(\alpha, f)|^2 \cdot G^{(m)}(\alpha, f)$  is calculated over measurement index  $m$ . The sAES can subsequently be used for automatic fault detection by searching for cyclic orders where  $\text{sAES}^{(i)}(\alpha) > 0$  and if the kinematics of the drive train are known, it would also be possible to identify the damaged component.

Lastly, the sAES can be used to obtain a simple Condition Indicator (CI) for time step  $i$  as follows:

$$\text{CI}_i = \frac{1}{\alpha_{max}} \int_0^{\alpha_{max}} \text{sAES}^{(i)}(\alpha) d\alpha, \quad (12)$$

with  $\text{CI}_i > 0$  indicates that anomalous behaviour is present, while  $\text{CI}_i = 0$  indicates that the spectral coherence of the measurement at time step  $i$  displays healthy behaviour. Since the smoothing operation removes the spurious anomalous components, the threshold can be set to  $\text{CI}_i = 0$  for detecting anomalous behaviour, which is used in the investigations of this paper. It is also possible to investigate other blind features such as the L2/L1 ratio [24] or the spectral negentropy [25] of the AES, but the optimisation of the condition indicator and the threshold selection is not considered in this work.

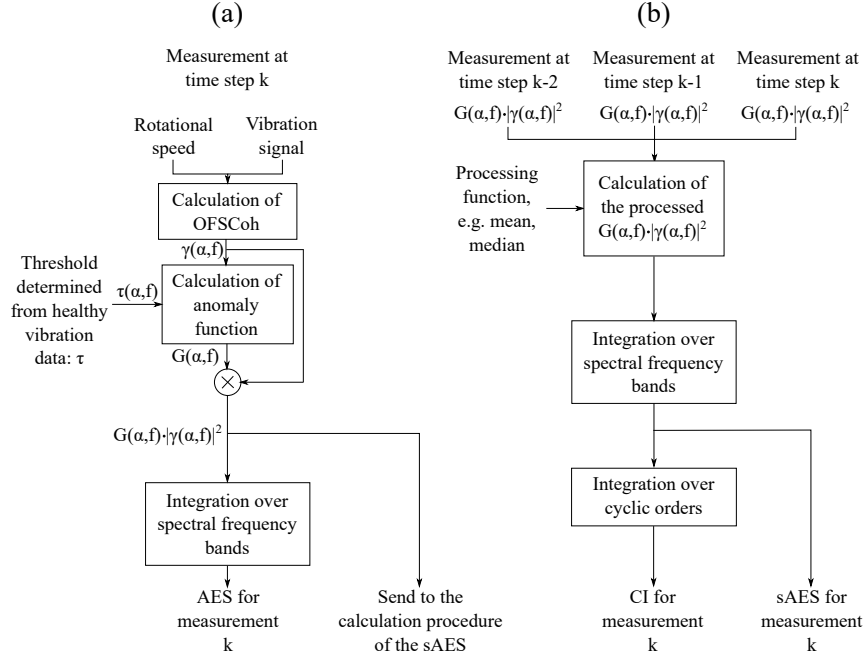


Figure 1: The calculation procedure of the Anomalous Envelope Spectrum (AES) for measurement  $k$  is shown in (a), while the calculation procedure of the smoothed AES (sAES) and its corresponding Condition Indicator (CI) are shown at time step  $k$  by using the information from the previous 3 time steps, i.e.  $N_s = 3$  in Equation (11).

#### 2.4. Summary

The calculation procedures of the AES and the sAES that were described in the previous sections are summarised in Figures 1(a) and 1(b) for time step  $k$ . The following parameters are used in all investigations:

- The median is used as the processing function  $\mathcal{P}$  in Equation (11). The median is much more robust to outliers than the mean and can therefore provide a more reliable estimate of the actual condition of the machine.
- The number of measurements used in calculating the sAES, i.e.  $N_s$  in Equation (11), is set to  $N_s = 10$ .
- The percentile  $\epsilon$  and the factor  $\kappa$  in Equation (10) are set to  $\epsilon = 95$  and  $\kappa = 4$ , respectively. The 95 percentile is used, because it is assumed that the healthy dataset does not contain much outliers and we desire to utilise the full distribution for detecting outliers in the damaged signal. We have found that  $\kappa = 4$  ensures that

1  
2  
3 the method is not too sensitive to outliers attributed to noise in the data and can  
4  
5 therefore result in less false alarms, while still performing very well in fault detection  
6  
7 and fault trending. The  $\kappa$  is further motivated in Section 4.2 and Appendix A.  
8  
9

10 This method is firstly investigated on numerical gearbox data in the next section, where-  
11  
12 after the method is investigated on three experimental gearbox datasets in Section 4.  
13  
14

### 15 16 **3. Numerical gearbox investigation** 17

18  
19 The phenomenological gearbox model presented in Ref. [4] is considered in this work  
20  
21 to simulate vibration data acquired from a gearbox operating under time-varying speed  
22  
23 conditions. The measured casing vibration signal of the gearbox in its reference condition  
24  
25

$$26 \quad x_c(t) = x_{gmc}(t) + x_{dgd}(t) + x_n(t), \quad (13)$$

27  
28  
29  
30 is decomposed in terms of three components, namely, a deterministic gear mesh component  
31  
32 denoted  $x_{gmc}(t)$ , a random gear component attributed to distributed gear damage denoted  
33  
34 by  $x_{dgd}(t)$  and a broadband noise component denoted by  $x_n(t)$ . Forty measurements  
35  
36 were taken from the gearbox in its reference condition, whereafter an additional signal  
37  
38 component due to outer race bearing damage is added to the casing vibration signal. The  
39  
40 new casing vibration signal  
41  
42

$$43 \quad x_c(t) = x_{gmc}(t) + x_b(t) + x_{dgd}(t) + x_n(t), \quad (14)$$

44  
45  
46  
47  
48 contains the additional bearing damage component denoted  $x_b(t)$ . More information re-  
49  
50 garding the signal components is given in Appendix B. Two-hundred measurements from  
51  
52 the damaged gearbox are investigated in this section, with the magnitude of the bear-  
53  
54 ing component increasing monotonically with the measurement number as discussed in  
55  
56 Appendix B and shown in Figure B.20.  
57  
58

59 The time-varying rotational speed profiles that were used to generate the vibration  
60  
61  
62  
63  
64  
65

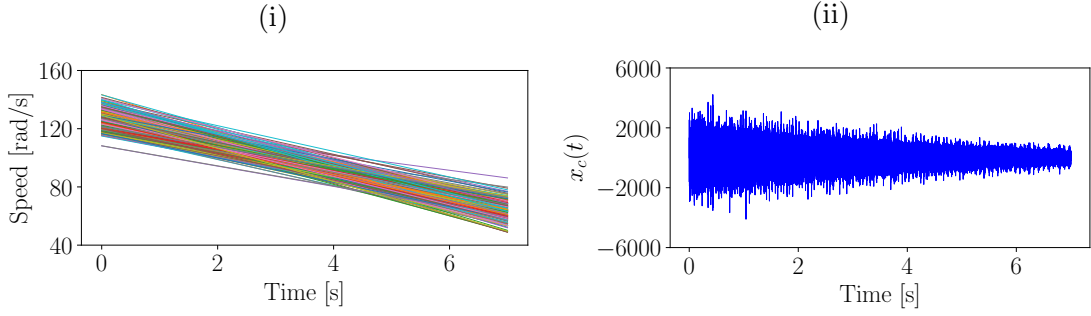


Figure 2: The rotational speeds that are under consideration in the phenomenological gearbox data as well as the vibration signal corresponding to the 110th measurement of the damaged gearbox.

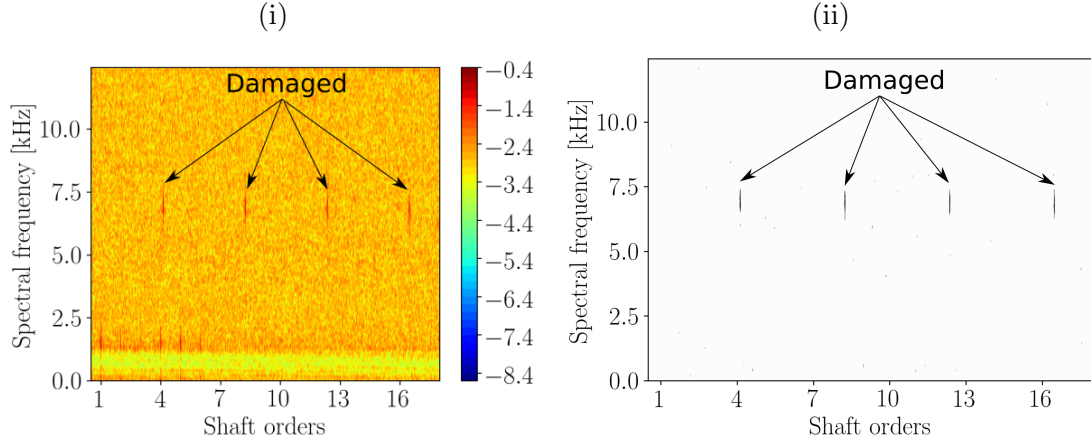


Figure 3: The OFSCoh of the vibration signal is presented in Figure 3(i) for the 110th measurement in the damaged dataset. The corresponding weighted OFSCoh is presented in Figure 3(ii).

data are presented in Figure 2(i). The casing vibration signal of the 110th measurement from the damaged gearbox (i.e. Equation (14)) shown in Figure 2(ii) is used to illustrate the different steps of the proposed method in this section.

The OFSCoh of the damaged gearbox is presented in Figure 3(i) for the measurement considered in Figure 2(ii). In Figure 3(i), the distributed gear damage component is clearly seen at a spectral frequency of 1.3 kHz and the components associated with the bearing damage are seen at 7 kHz. The methodology was applied on the 110th measurement of the considered dataset to obtain the resulting weighted OFSCoh, which is presented in Figure 3(ii). The weighted OFSCoh, calculated with  $G^{(i)}(\alpha, f) \cdot |\gamma^{(i)}(\alpha, f)|^2$ , only contains the bearing component at the spectral frequency of 7kHz, because the bearing damage

component is the only novel component in the signal. Hence, the weighted OFSCoh is able to enhance the novel components in the signal and attenuate the dominant components that were in the reference signal.

The integrated spectra, i.e. the EES, the AES and the sAES, are presented in Figure 4 for two measurements. No additional processing was performed before the EES and AES were calculated. The distributed gear damage component, with a cyclic order of 1.0 shaft orders, is dominant in the OFSCoh and therefore makes the weak bearing damage components more difficult to detect in the EES shown in Figure 4. Since both signals are random, they cannot be separated using techniques such as the generalised synchronous average [4]. In contrast to the EES, the bearing damage components are very prominent in the AES and the sAES, since the distributed gear damage components are removed in the weighted OFSCoh presented in Figure 3(ii). The sAES contains much less noise than the AES due to the additional processing that is performed.

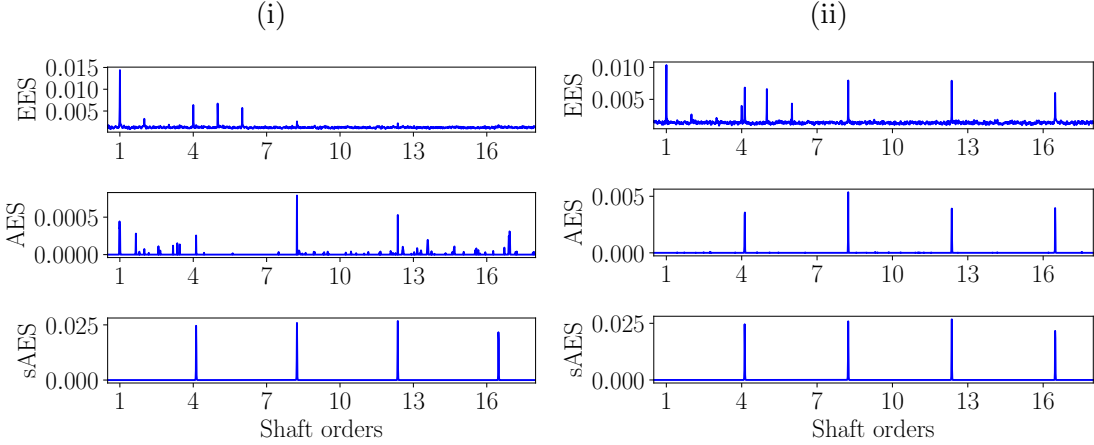


Figure 4: The integrated spectra are presented for two measurements in the damaged gearbox dataset. The integrated spectra of the 77th measurement and 110th measurement are presented in Figures 4(i) and 4(ii) respectively.

Since it is not only important to determine whether it is possible to detect bearing damage, but also whether changes in the condition can be detected, different magnitudes of bearing impulses are investigated. The magnitude of the bearing impulses were increased monotonically over the measurement number. Please refer to Figure B.20 for more infor-

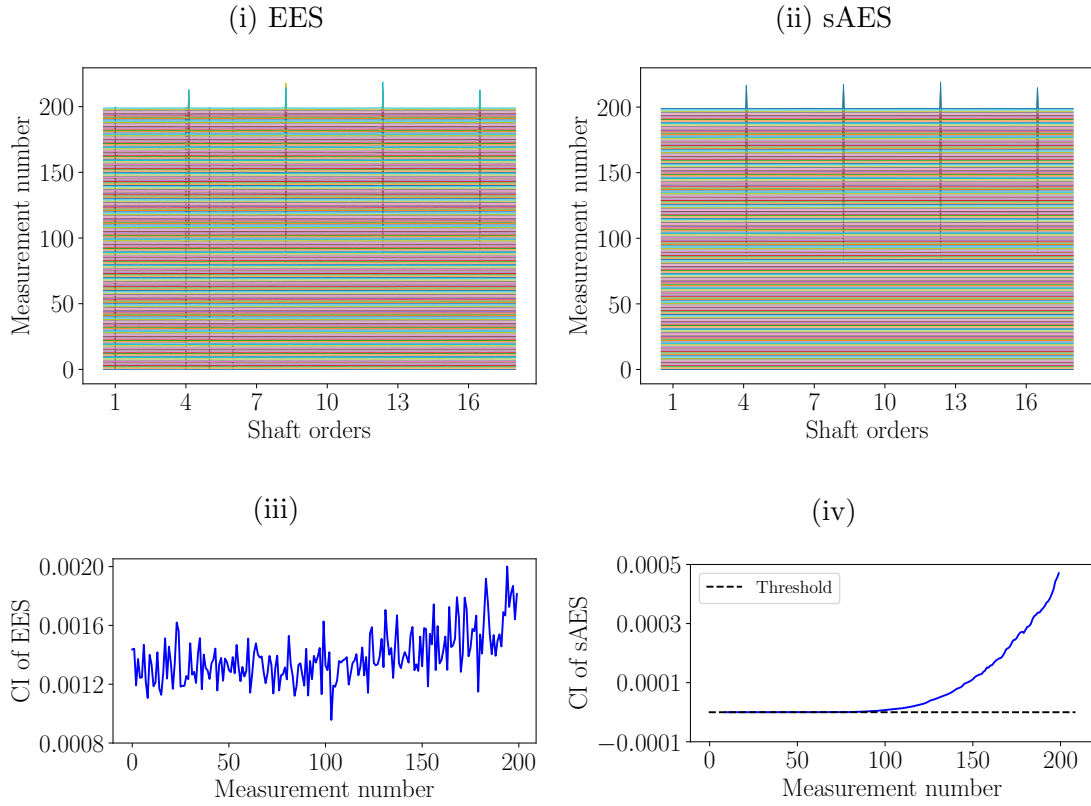


Figure 5: A waterfall plot of the EES and the sAES as well as their corresponding condition indicators are presented for the phenomenological gearbox model.

mation. The EES and the sAES of the different measurements under consideration are presented in Figures 5(i) and 5(ii), respectively. The exact signal-to-noise ratios of the bearing component for each measurement are included in Appendix B. The distributed gear damage and bearing damage components can be seen in the EES presented in Figure 5(i), while the sAES does not contain any signal components until the bearing damage component is detected. The bearing damage components at 4.12 shaft orders and its harmonics are clearly seen.

The mean of the integrated spectra are investigated as condition indicators for fault trending. The mean of the EES and the mean of the sAES as calculated with Equation (12) are presented in Figures 5(iii) and 5(iv) respectively. The condition indicator of the EES contains much noise which makes it difficult to observe the increase of the condition indicator due to the change in the magnitude of the bearing component. However, the CI

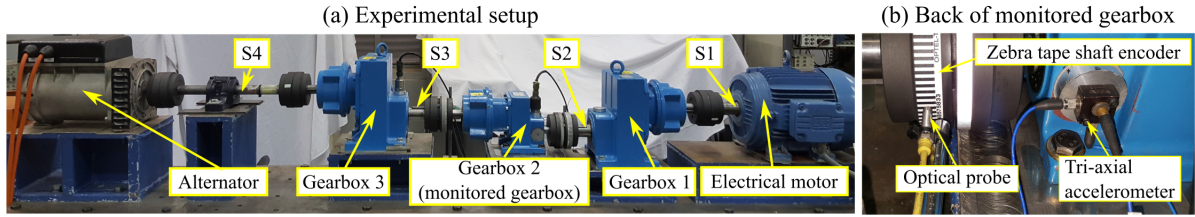


Figure 6: The experimental setup with the important components and parts highlighted.

of the sAES performs much better, due to the fact that it is not affected by the noise in the signal and provides a monotonic trend which is consistent with the magnitude of the bearing impulses that increases monotonically over the measurement number.

Hence, the proposed anomalous envelope spectrum and its related metrics are not only capable of detecting changes in the condition of the bearing, but it is also able to identify at which cyclic orders the damage manifests when inspecting the sAES. In the next section, the proposed method is investigated on experimental data.

#### 4. Experimental gearbox investigation

The proposed method is now investigated on experimental data that were acquired from a helical gearbox under time-varying operating conditions. In Section 4.1, an overview of the experimental setups and the measurement equipment is given, whereafter measurements taken from a gearbox with localised gear damage are investigated in Section 4.2 and measurements taken from a gearbox with distributed gear damage are investigated in Section 4.3. Finally, the method is investigated on healthy gearbox data in Section 4.4.

##### 4.1. Experimental setup

The data considered in this section were acquired from the experimental setup shown in Figure 6. The experimental setup consists of three helical gearboxes, an alternator and an electrical motor. The shafts between the different components are denoted by S1, S2, S3 and S4 respectively. The centre helical gearbox is monitored for damage with two accelerometers, namely, a single-axis accelerometer and a tri-axial accelerometer. The methodology is applied on the axial-component of the tri-axial accelerometer, which is



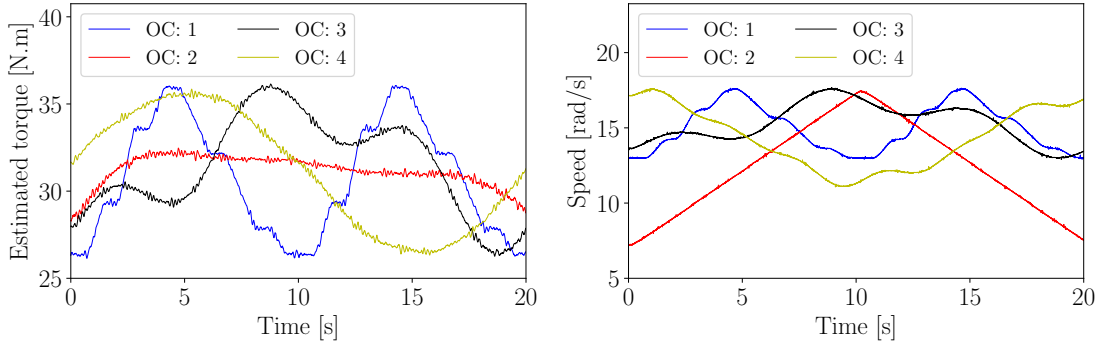


Figure 7: The operating conditions that were estimated at the input shaft of the gearbox, i.e.  $S_2$  in Figure 6.

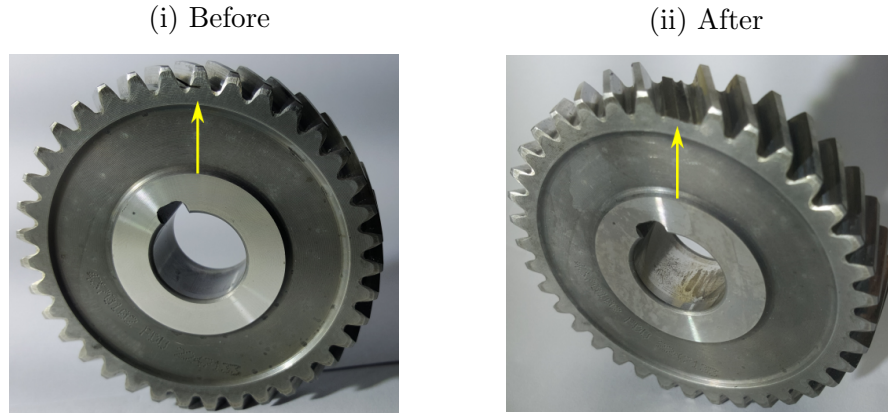
located on the bearing housing of the monitored gearbox as seen in Figure 6(b). The instantaneous speed of the input shaft of the gearbox (i.e.  $S_2$  in Figure 6) was measured with the optical probe and the zebra tape shaft encoder also shown in Figure 6(b). An OROS OR 35 data acquisition device was used with an accelerometer signal that was sampled at a rate of 25.6 kHz, while the optical probe was sampled at 51.2 kHz.

The electrical motor and the alternator were independently controlled to apply the time-varying operating conditions to the monitored gearbox as shown in Figure 7.

The monitored helical gearbox in Figure 6 consists of a gear and a pinion. The pinion was kept healthy for all measurements, while the gear was damaged as discussed in the next sections. Since the gear is connected to the reference shaft  $S_2$  in Figure 6, it rotates at 1.0 shaft order. This means that impacts from a damaged gear tooth would modulate the signal at 1.0 shaft order and would therefore be detected at 1.0 shaft order and its harmonics when interrogating the envelope spectrum. In Appendix C, the RMS, the kurtosis and the L2/L1-norm ratio of the SES are presented for the raw vibration signals considered in this work. This is to further highlight the benefits of using the proposed method.

#### 4.2. Localised gear damage experiment

Localised gear damage such as root cracks can severely affect the remaining useful life of gearboxes and is therefore very important to detect. An experiment was firstly performed with both gears of the monitored gearbox being healthy. Forty measurements, taken while



17  
18  
19  
20  
21

Figure 8: The gear with localised gear damage is presented. In Figure 8(i), the gear before the fatigue experiment is presented, while in Figure 8(ii) the gear after the fatigue experiment is presented. The seeded slot was 50% of the tooth thickness deep and had a height of 0.3 mm.

22  
23  
24  
25  
26  
27  
28  
29  
30  
31  
32  
33  
34  
35  
36  
37  
38  
39  
40  
41  
42

the gearbox was operating under operating condition 1 in Figure 7, are used to calculate the bivariate threshold function  $\tau(\alpha, f)$  with Equation (10). Thereafter, the gearbox was disassembled and the gear was damaged by seeding a small slot in the root of the gear tooth as shown in Figure 8(i). The helical gears have much larger contact ratios than spur gears and vibration signals contain impulsive components that make the gear damage shown in Figure 8(i) more difficult to detect. The monitored gearbox was reassembled with the damaged gear and tested for approximately 20 days under operating condition 1 before the damaged tooth failed as shown in Figure 8(ii). Two-hundred measurements, approximately evenly spaced over the testing period, are used to evaluate the effectiveness of this methodology.

43  
44  
45  
46  
47  
48  
49  
50  
51  
52  
53  
54  
55  
56  
57  
58  
59  
60  
61  
62  
63  
64  
65

However, this experiment does not represent the actual conditions that would be expected in a real application. If maintenance is performed on the system, the damaged components would be replaced with healthy components, which would make new measurements available for calculating the threshold  $\tau$ . In this experiment, we needed to replace the gear with a damaged gear to ensure that the gear would fail in a reasonable time. The implication of this is that there may be some differences between the experimental setup under consideration and the reference experimental setup which could also result in the measurements to have different statistical properties. Hence,  $\kappa$  in Equation (10) was made sufficiently large (i.e.  $\kappa = 4$ ) to ensure that false alarms are avoided.

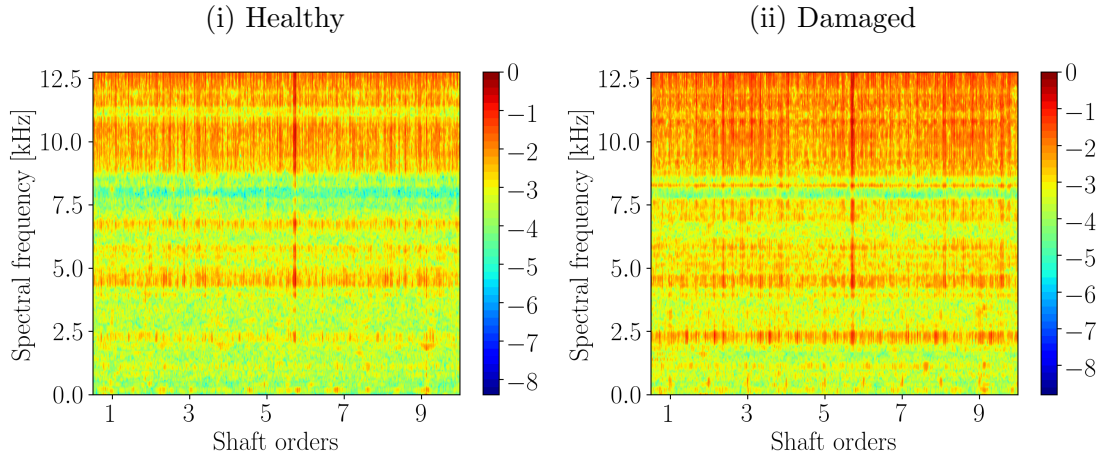


Figure 9: The logarithm of the mean OFSCoh of the healthy data and the logarithm of the OFSCoh from a damaged signal are presented in Figures 9(i) and 9(ii) on different colour scales.

The average spectral coherences of the healthy measurements are presented in Figure 9(i) to emphasise the motivation of using a bivariate threshold  $\tau(\alpha, f)$  in the method. If the threshold was set to a constant value for all cyclic orders and spectral frequencies, it may be too sensitive to noise at specific combinations of  $\alpha$  and  $f$ , while being insensitive to damage at other combinations of  $\alpha$  and  $f$ . The OFSCoh of one of the measurements from the damaged gearbox is presented in Figure 9(ii). The damaged components are located in a resonance band at approximately 500 Hz, but the OFSCoh is dominated by other phenomena which make the damage difficult to detect.

The corresponding weighted OFSCoh is presented in Figure 10(i). Since the impacts attributed to localised gear damage are the only new information in the signal, the weighted OFSCoh retains only the damaged information in the aforementioned frequency bands as seen in Figure 10(i). Since the damage only manifest in a very localised region of the OFSCoh, a zoomed view is included in Figure 10(i). Lastly, the different integrated OFSCoh of the measurement from the damaged gearbox are presented in Figure 10(ii). The EES only retains a strong component at 5.72 shaft orders, but the components attributed to the gear damage cannot be clearly seen. The AES and the sAES perform much better, because they are able to identify the damaged components in the signal, with the sAES containing a much clearer representation due to the additional processing that is

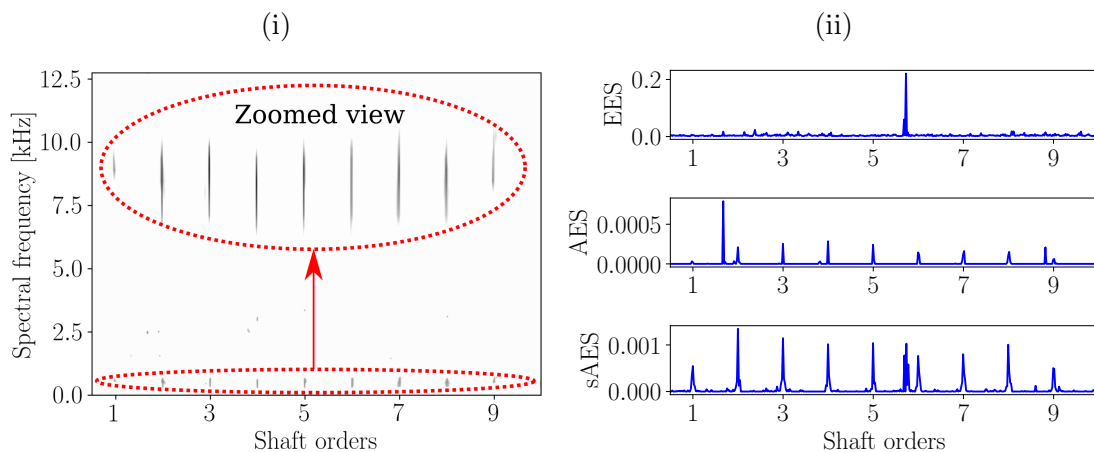


Figure 10: The weighted OFSCoh and corresponding integrated spectra are presented for the same signal considered in Figure 9(ii).

performed. Hence, it is clear that the proposed method is a very powerful representation for identifying frequency bands with novel information and using this not only for fault detection, but also for fault identification.

The EES and the sAES are presented over the measurement number in Figure 11. The EES contains the very strong component at 5.72 shaft orders for all measurements, while being unable to detect the damaged gear component. This dominant impulsive signal component is present in both the healthy and the damaged datasets, however, it impedes the detection of the damaged gear component. The signal component at 5.72 shaft orders is attributed to the movement of the floating shaft in the monitored gearbox that results in undesired contact between the bearing and the casing of the gearbox. The movement is exacerbated by the fact that the input shaft of the helical gearbox has strong axial excitations due to the axial forces of the helical gears.

In contrast, the sAES performs much better than the EES. In the sAES in Figure 11, the signal components associated with the damaged gear are very prominent in the spectrum, while it is also possible to see the degradation of the components over time as the condition of the gear worsens. Lastly, the Condition Indicator (CI) is calculated from the EES and the sAES and presented in Figure 12 over the measurement number. It is not possible to see the deterioration of the gear in the EES feature, because the signal-to-

1  
2  
3  
4  
5  
6  
7  
8  
9  
10  
11  
12  
13  
14  
15  
16  
17  
18  
19  
20  
21  
22  
23  
24  
25  
26  
27  
28  
29  
30  
31  
32  
33  
34  
35  
36  
37  
38  
39  
40  
41  
42  
43  
44  
45  
46  
47  
48  
49  
50  
51  
52  
53  
54  
55  
56  
57  
58  
59  
60  
61  
62  
63  
64  
65

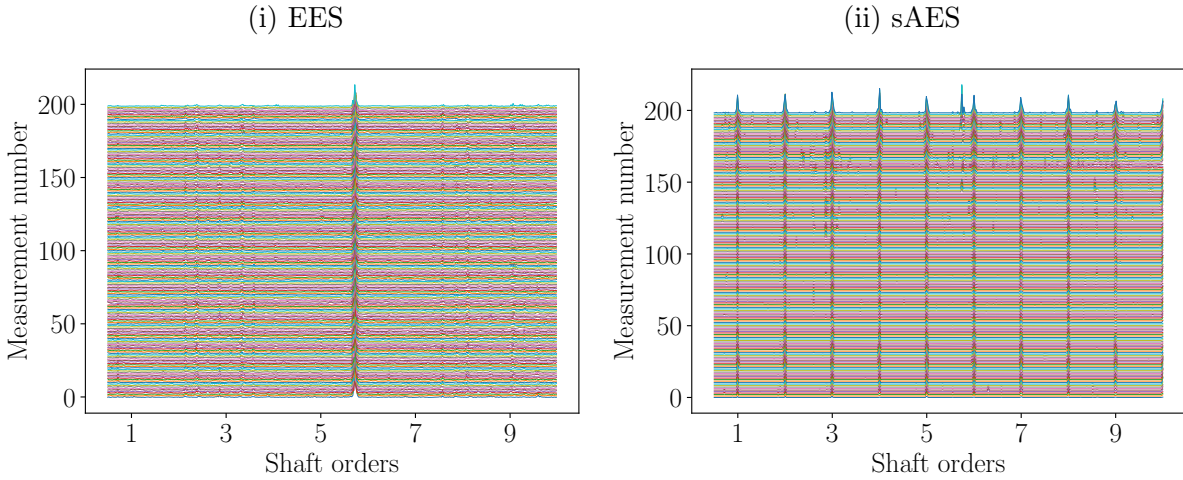


Figure 11: The Enhanced Envelope Spectra (EES) and the smoothed Anomalous Envelope Spectrum (sAES) of the data acquired from the gearbox with localised gear damage.

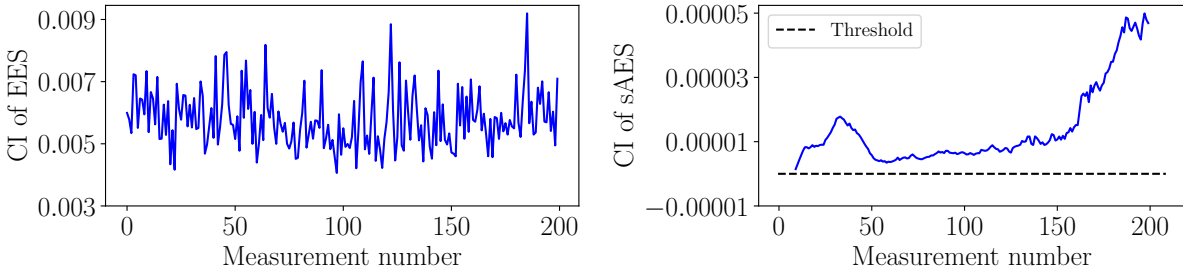


Figure 12: The blind condition indicators of the EES and the sAES are presented over measurement number.

noise ratios of the damaged components are too low in the EES. This is in contrast to the sAES. The CI associated with the sAES is always larger than zero, which indicates that the system contains anomalous information. Initially the CI makes a hump between the first and the 50th measurements, whereafter the CI steadily increases until the gear failed. We do not know the reason behind the hump in the CI at the start of the experiment, since the gearbox was not opened nor inspected between the start of the measurement and the end of the experiment. However, we speculate that this was due to propagation of the gear damage starting in the initial measurements, whereafter it stabilised until the crack reached its critical length.

Comparing the results against the results obtained with the raw signal in Appendix C, it is evident that the proposed method highlights the fault information in the vibration

1  
2  
3 signal and makes it possible to see the degrading gear component.  
4  
5

#### 6 *4.3. Distributed gear damage experiment* 7

8  
9 Distributed gear damage modes such as pitting are very frequently encountered in crit-  
10 ical rotating machines such as wind turbine gearboxes [26]. The distributed gear damage  
11 can result in localised gear damage to develop, which could lead to the failure of the gear-  
12 box. Hence, distributed gear damage is also very important to detect, especially under  
13 time-varying operating conditions.  
14  
15  
16  
17  
18

19 The gear of the monitored gearbox was replaced with a healthy gear and tested again.  
20 In the healthy and the testing dataset all operating conditions in Figure 7 are considered.  
21 Forty measurements were again taken from the healthy gearbox whereafter the gearbox  
22 was disassembled and replaced with a different gear that was left in a corrosive environment  
23 for a long time. This gear is presented in Figure 13(a), where the surface damage is clearly  
24 seen. The damaged gear was tested for approximately eight days before the experiment  
25 was stopped due to excessive vibrations that were measured on the gearbox. This damaged  
26 gear after the completion of the experiment is presented in Figure 13(b). After inspecting  
27 the data, it was observed that the gear experienced a tooth failure at approximately the  
28 100th measurement of the 200 considered in this work, which resulted in the higher loads  
29 and impacts on the adjacent teeth. This subsequently resulted in the adjacent gear teeth  
30 to fail in the final stages of the test.  
31  
32  
33  
34  
35  
36  
37  
38  
39  
40  
41  
42  
43

44 The methodology is again similarly applied as in the previous section, where a threshold  
45  $\tau(\alpha, f)$  is obtained of the healthy data, which is subsequently used to calculate the AES  
46 and the sAES. The 200 measurements that were acquired over the life of the gear are  
47 presented in Figure 14 for the EES and the sAES. Both the EES and the SAES are able to  
48 detect the gear damage components at 1.0 shaft orders and its harmonics, but the sAES  
49 contains much lower noise levels. The benefit of the lower noise levels is highlighted when  
50 investigating the condition indicator of the EES and the sAES.  
51  
52  
53  
54  
55  
56  
57  
58

59 The condition indicators of the EES in Figure 15 contains much noise and it is difficult  
60  
61  
62  
63  
64  
65



(a) Before the experiment started

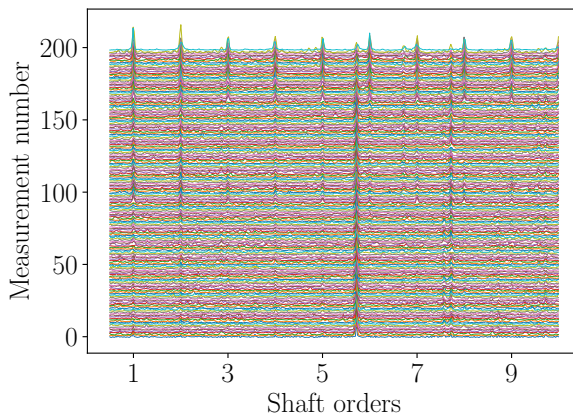


(b) After the experiment was completed



Figure 13: The gear before the experiment started and after the experiment was completed are presented in Figures 13(a) and 13(b) respectively. The damaged regions of the gear are clearly highlighted in Figure 13(b).

(i) EES



(ii) sAES

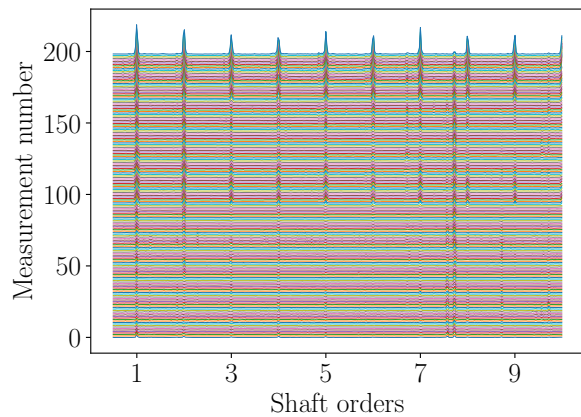


Figure 14: The Enhanced Envelope Spectra (EES) and the smoothed Anomalous Envelope Spectrum (sAES) of the vibration data acquired during the distributed gear damage experiment.

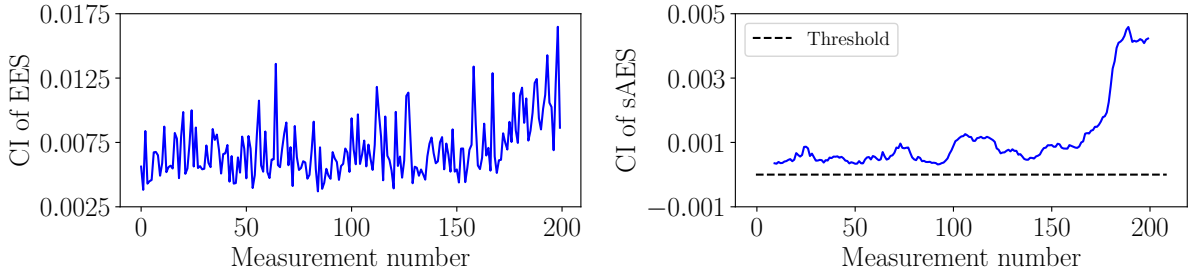


Figure 15: The blind condition indicators calculated with the EES and the sAES are presented over measurement number for the distributed gear damage experiment.

to detect the deterioration of the gear over time. This is in contrast to the results obtained with the sAES condition indicator that is presented in Figure 15. The CI of the sAES is clearly larger than the threshold, which is indicative that the gearbox contains anomalous behaviour. The changes of the CI of the sAES over time, indicates the degradation of the gear, with the two events associated with the failure of the gear teeth seen at approximately the 100th measurement number and the 175th measurement respectively. Hence, the proposed method results in a significant improvement.

The sAES is therefore very capable of not only detecting that there is damage present in the system, but it is also possible to determine the cyclic orders of the anomalous component that is changing over time.

#### 4.4. Healthy gearbox

Vibration data from a healthy gearbox are investigated in this section. This vibration data were not used for estimating the threshold  $\tau(\alpha, f)$ , i.e. we did not use the training data. The integrated spectra (i.e. EES, AES and sAES) are presented for two measurements of the healthy gearbox in Figure 16. The EES is dominated by the 5.72 shaft orders component. The AES contains spurious anomalous components at different cyclic orders, however, these components are random and are removed in the smoothing process as shown in the sAES. The spurious components are attributed to the vibration data from the gearbox being random and the OFSCoh being very sensitive to weak components.

The condition indicators associated with the EES and the sAES are also presented in Figure 16. The EES contains some random fluctuations, but does not have an increasing



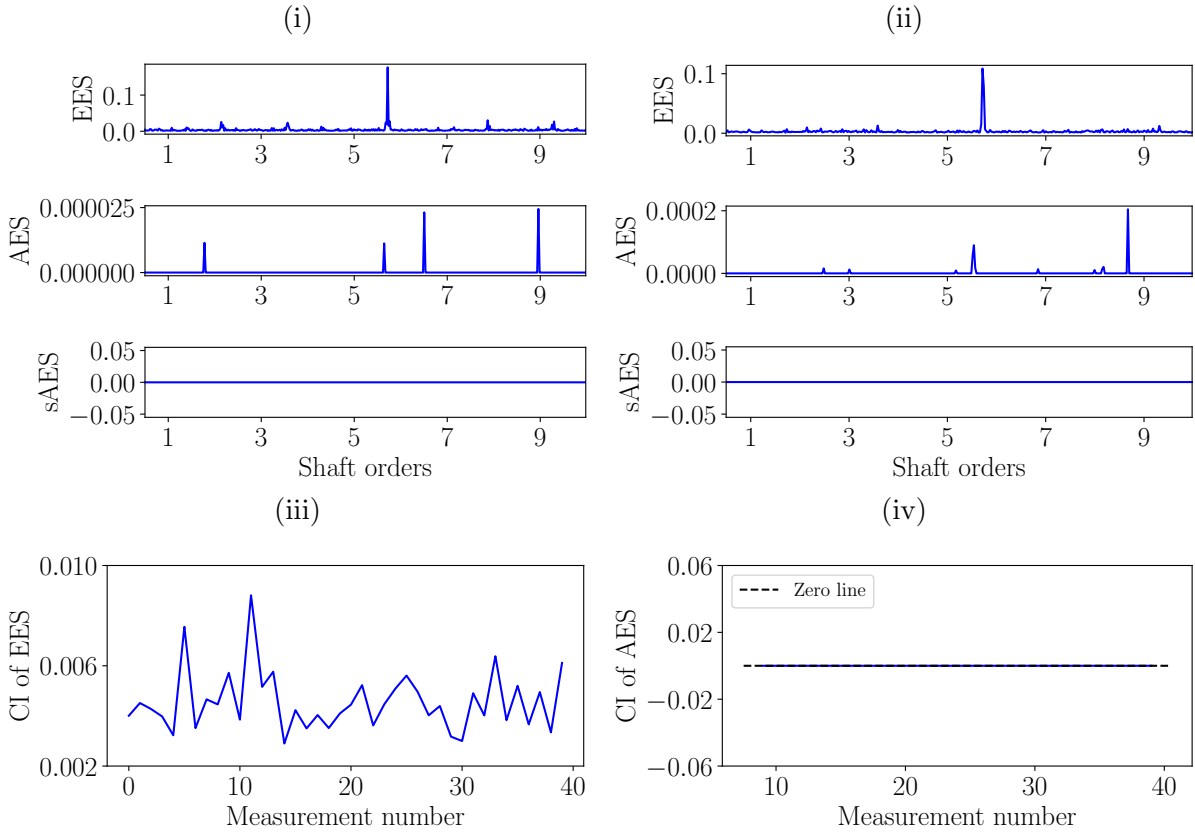


Figure 16: The Enhanced Envelope Spectra (EES) and the smoothed Anomalous Envelope Spectrum (sAES) and their corresponding condition indicators are presented for the vibration data acquired from a healthy gearbox. The healthy gearbox data were acquired from a different experiment compared to the data used in the training procedure.

trend. In contrast the sAES is 0 for all measurements. This is attributed to the removal of the dominant healthy components by the AES, whereafter the smoothing operation removes the spurious noise components. The results therefore indicate that the proposed method allows us to distinguish between a healthy gearbox and a damaged gearbox.

## 5. Additional considerations of the proposed method

Two important aspects of the proposed method are considered in this section, namely,

- the average time required to calculate the AES and sAES; and
- the amount of historical data required to estimate a suitable threshold.

### 5.1. Average calculation time

The average time to perform the different steps of the proposed method is summarised

in Table 1 for the numerical and the experimental gearbox datasets. The bottleneck in the proposed method is caused by the calculation of the OFSCoh, which is attributed to the Welch-based estimator being used to estimate the OFSCoh. As mentioned in Section 2.1, there are much faster estimators available to calculate the spectral coherence (e.g. [11, 20]) and should be used to reduce the time needed to calculate the AES and the sAES. The Table 1: The average time in seconds to perform the different steps is included. This was performed with a personal computer with 32 Gb of RAM and an AMD Ryzen 7 2700x eight-core processor. Python 3.7.3 was used with NumPy 1.16.4 and SciPy 1.3.0.

Description	Numerical	Experimental
OFSCoh	1193.0918 [s]	325.72 [s]
Weighted OFSCoh	1.22617 [s]	0.2655 [s]
AES and sAES	0.10213 [s]	0.02330 [s]

numerical gearbox dataset took longer to calculate because the OFSCoh matrix was larger than the experimental dataset. This is attributed to the higher rotational speeds, which required a finer cyclic order resolution; and the OFSCoh of the numerical dataset had to include higher cyclic orders due to the higher characteristic orders of the components of interest. The EES, IES, and the IESFOgram [23] would also be calculated from the estimated OFSCoh and therefore the calculation time is expected to be the same order of magnitude.

5.2. Influence of the historical data

The proposed method is a novelty enhancement method and has two important aspects that need to be considered:

- The quality of the historical data for calculating the threshold.
- The amount of historical data that is necessary to calculate the threshold.

This method relies on the threshold for identifying anomalous components in the order-frequency spectral coherence. Similarly to novelty detection and semi-supervised learning methods, this threshold is estimated with the available historical data and therefore the quality of the historical data (e.g. amount of historical data, representation of the healthy

1  
2  
3 system, presence of outliers) would influence the detection of anomalous components.  
4  
5 Hence, the quality of the historical data would directly influence the performance of the  
6  
7 method, e.g. the method could be either too sensitive to extraneous components and  
8  
9 result in many false positives or be insensitive to damage and therefore result in the  
10  
11 damage to be detected too late. Therefore, we recommend that a large number of healthy  
12  
13 data files are measured to ensure a good estimate of the threshold is obtained. After the  
14  
15 measurements are acquired from the healthy system, it is recommended that the threshold  
16  
17 is estimated and used to monitor the system. This would ensure that the threshold is a  
18  
19 good representation of the healthy system and would allow changes from the healthy  
20  
21 system to be detected.  
22

23  
24 The influence of the number of healthy files on the resulting condition indicator is  
25  
26 shown in Figure 17 for the simulated data. In each sub-figure, a constant number of  
27  
28 healthy files are used, with 10 batches randomly sampled for the 20 and 30 file cases. This  
29  
30 allows us to showcase the variation in the performance of the method. The variation is not  
31  
32 significant between different batches of healthy measurements, since the simulated data  
33  
34 are very well-behaved, i.e. the generative distribution of the healthy data is the similar  
35  
36 between healthy measurements. This is in contrast to experimental measurements that  
37  
38 could contain additional variations due to environmental changes (e.g. temperature) for  
39  
40 example.  
41

42  
43 The same investigation is performed for the experimental dataset where localised dam-  
44  
45 age was introduced in the tooth of the gear of the system. The results are presented in  
46  
47 Figure 18, with the influence of the number of files being much more prominent. For  
48  
49 example, if 20 files are used to obtain the threshold, a significant variation is observed.  
50  
51 This is attributed to the fact that the number of files is small and that variations between  
52  
53 measurements (e.g. changes in environmental temperatures) could have affected the re-  
54  
55 sults. Hence, it is concluded that 20 measurements are insufficient and more measurements  
56  
57 should be used to reduce the variance of the estimators.  
58  
59  
60  
61  
62

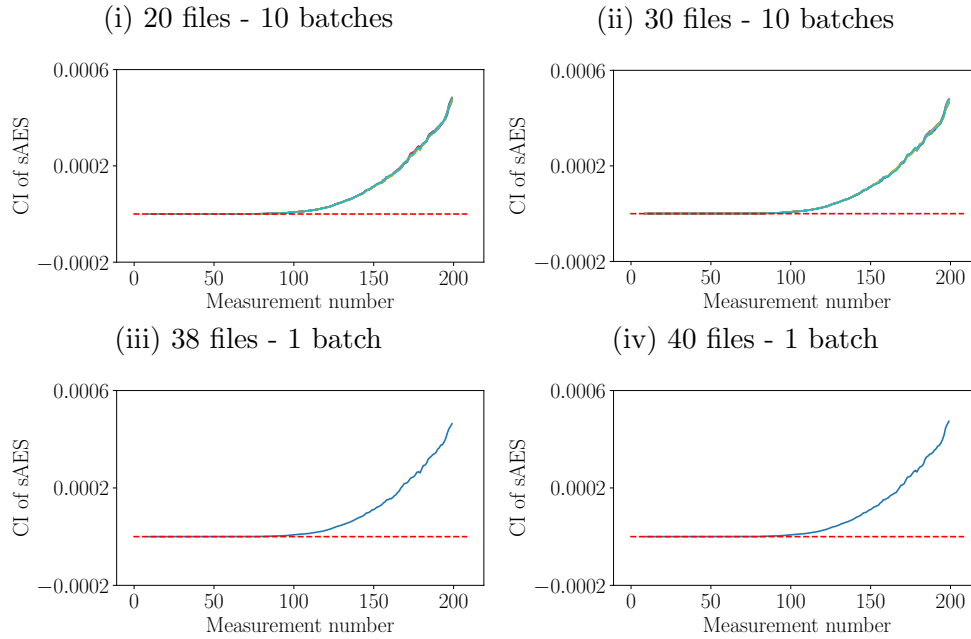


Figure 17: The influence of the number of training files on the condition indicator. Multiple lines on the same plot indicates cases where different batches of the healthy dataset were used.

## 6. Conclusions and recommendations

A new methodology is proposed in this work to perform fault diagnosis under time-varying operating conditions. This methodology does not require much knowledge about the kinematics of the machine (i.e. it is blind) nor much human effort to interrogate the results. In this methodology, the order-frequency spectral coherence and healthy historical data are used to calculate an anomalous envelope spectrum, a smoothed anomalous envelope spectrum and a condition indicator. These representations can be used for not only detecting damage in the rotating machine, but it can also be used to identify the damaged components and be used to perform fault trending. The methodology is investigated on a numerical gearbox dataset and three experimental datasets, where it is shown that the proposed method has much potential for performing condition monitoring under time-varying operating conditions.

Future work would investigate and compare different methods of modelling the healthy spectral coherences under time-varying operating conditions (e.g. different threshold selection procedures); different blind condition indicators that can be extracted from the

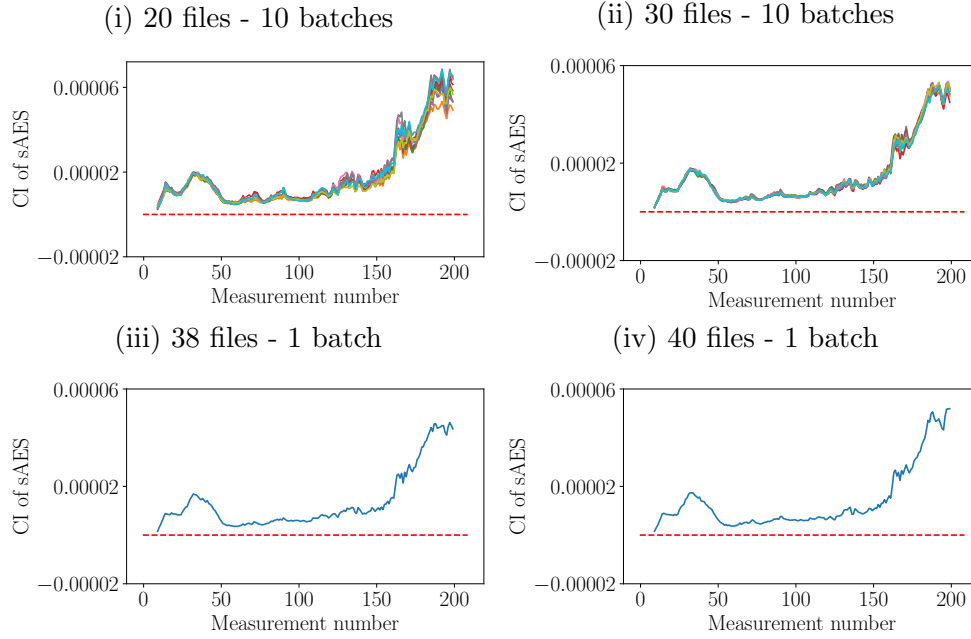


Figure 18: The influence of the number of training files on the condition indicator of the localised gear damage experiment. Multiple lines on the same plot indicates cases where different batches of the healthy dataset were used.

anomalous envelope spectrum; and also recalibration procedures of the threshold if the gearbox was assembled and disassembled during the monitoring period. Since the calculation time of the proposed method is governed by the calculation of the order-frequency spectral coherence, the performance of the method using faster estimators will be considered in future work.

## Appendix A. Threshold selection motivation

If the  $\xi$ th percentile is used in Equation (10) with  $\kappa = 1$  there would be  $100 - \xi\%$  false positives during monitoring. This would therefore result in regular false alarms and should be avoided. The number of false positives can be reduced by selecting  $\kappa > 1$ . In general, care should be taken when selecting  $\kappa > 1$  as this result in extrapolation. However, this is sensible for this application, because of the following reasons:

- The OFSCoh is very sensitive to weak components and therefore large changes are expected in the OFSCoh if damage is present, i.e. it would exceed the threshold even if  $\kappa > 1$ .

- The distribution of the OFSCoh is known to be chi-squared distributed [7, 10].

In Figure A.19(i), the false positive rates are presented as a function of  $\kappa$  for different distributions. The probability distribution of the OFSCoh is expected to be chi-squared distributed with two degrees-of-freedom if the length of the signal is very long [7, 10] and it is not expected to be uniform, Gaussian or Laplacian distributed. If  $\kappa = 4$ , then very few false positives are expected. However, since the OFSCoh is very sensitive to weak damage components, it will still make it possible to detect the damaged components. This is proven by the results in the main document.

Ultimately, the threshold is estimated from a limited number of healthy measurements. This makes the threshold  $\tau$  a random variable with an underlying sampling distribution. In Figure A.19(ii), the results are presented for the case where we use the 5th and 95th percentile of the sampling distribution of  $\tau$  as a threshold. The performance of the method is clearly dependent on the number of measurements that are used to estimate the threshold. However, by using  $\kappa = 4$  on the OFSCoh data, the results are deemed sufficient for this paper.

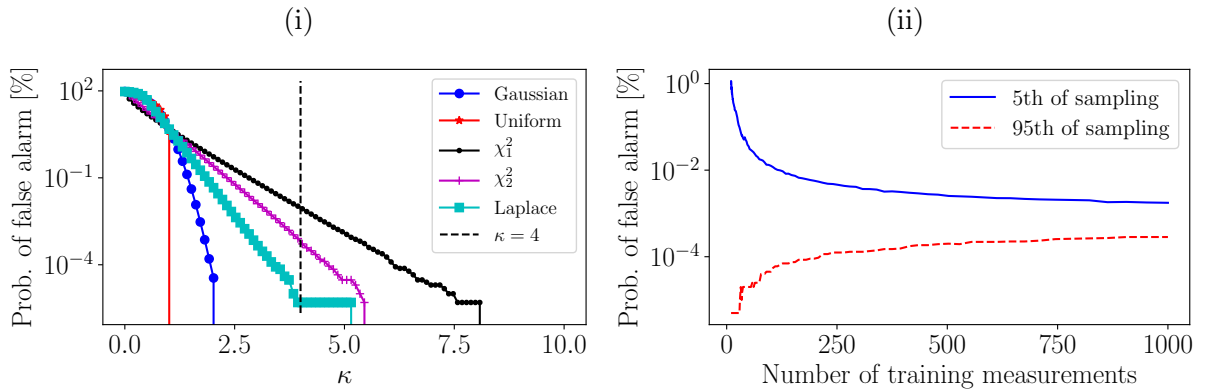


Figure A.19: In Figure A.19(i) the probability of a false alarm is presented for different distributions, calculated using samples from the same distribution as a function of  $\kappa$  in Equation (10). In Figure A.19(ii), the probability of a false alarm is presented for a chi-squared distribution for two degrees of freedom as a function of  $N$  using the 5th and 95th percentile of the sampling distribution for calculating the threshold. This illustrates the variance in the results that can be expected when using a limited number of samples for estimating the threshold  $\tau$  with  $\kappa = 4$ .

## Appendix B. Phenomenological gearbox model

The model used in this work is based on the model used in Ref. [4]. However, it is important to summarise the signal components for understanding the model. The casing vibration signal of the gearbox with bearing damage can be decomposed as

$$x_c(t) = x_{gmc}(t) + x_{dgd}(t) + x_b(t) + x_n(t), \quad (\text{B.1})$$

The gear mesh component is attributed to the deterministic gear mesh interactions and is calculated with

$$x_{gmc}(t) = M(\omega(t)) \cdot h_{gmc}(t) \otimes \left( \sum_{k=1}^{N_{gmc}} A_{gmc}^{(k)} \cdot \sin \left( k \cdot N_{teeth} \cdot \int_0^t \omega(\tau) d\tau + \varphi_{gmc}^{(k)} \right) \right), \quad (\text{B.2})$$

where  $M(\omega(t)) = \omega^2$  simulates the dependence of the signal-component to rotational speed. The impulse response function  $h_{gmc}(t)$  is approximated with a single degree of freedom system with a natural frequency of 2000 Hz and a damping ratio of 0.05. The amplitude and phase of the  $i$ th gear mesh component are denoted by  $A_{gmc}^{(k)}$  and  $\varphi_{gmc}^{(k)}$  respectively. The instantaneous gear mesh frequency is calculated with  $N_{teeth} \cdot \omega(t)$ , where  $N_{teeth}$  is the number of teeth on the gear.

The random gear component is attributed to distributed gear damage and is calculated with

$$x_{dgd}(t) = M(\omega(t)) \cdot h_{dgd} \otimes \left( \varepsilon_\sigma(t) \cdot \sum_{k=1}^{N_{dgd}} A_{dgd}^{(k)} \cdot \sin \left( k \cdot \int_0^t \omega(\tau) d\tau + \varphi_{dgd}^{(k)} \right) \right), \quad (\text{B.3})$$

which has the same form as the gear mesh component, except for the additional variable  $\varepsilon_\sigma(t)$ . The variable  $\varepsilon_\sigma(t)$  is sampled from a standardised Gaussian and simulates the interactions between the damaged gear teeth during meshing. The single degree-of-freedom impulse response function of the distributed gear damage component  $h_{dgd}(t)$  has a natural frequency of 1300 Hz and a damping ratio of 0.05.

The broadband noise component is calculated with

$$x_n(t) = M(\omega(t)) \cdot \epsilon_\sigma(t) \quad (\text{B.4})$$

which consists of standardised Gaussian noise  $\epsilon_\sigma(t)$  being scaled by changes in rotational speed with  $M(\omega(t))$ .

Bearing damage on the outer race of a rolling element bearing would result in impacts as the rolling elements move in-and-through the defective area. These impacts result in broadband excitation of the structure as it is filtered from the source of the bearing damage through the structure to the transducers. The measured outer race bearing damage signal is simulated with

$$x_b(t) = M(\omega(t)) \cdot h_b(t) \otimes \left( \sum_{k=0}^{N_{imp}-1} A_b^{(k)} \cdot \delta(t - T_b^{(k)}) \right), \quad (\text{B.5})$$

where the impulse response function of the bearing damage component  $h_b(t)$  has a natural frequency of 7000 Hz and a damping ratio of 0.05. The signal contains  $N_{imp}$  impulses, with the  $k$ th impulse having a time-of-arrival given by  $T_b^{(k)}$  and its magnitude is scaled with  $A_b^{(k)}$ .

Since it is desired to investigate the ability of the proposed method to perform fault trending the magnitude of the bearing damage component is scaled as shown in Figure B.20. The RMS of the resulting bearing signals are also presented over measurement number.

### Appendix C. Experimental results

The root-mean-square of the raw vibration signal; the kurtosis of the raw vibration signal; and the L2/L1 norm ratio of the SES of the raw order tracked signal are presented in Figure C.21. The RMS is very sensitive to time-varying operating conditions and does not clearly indicate that the gear is damaged for the localised gear and distributed gear damage



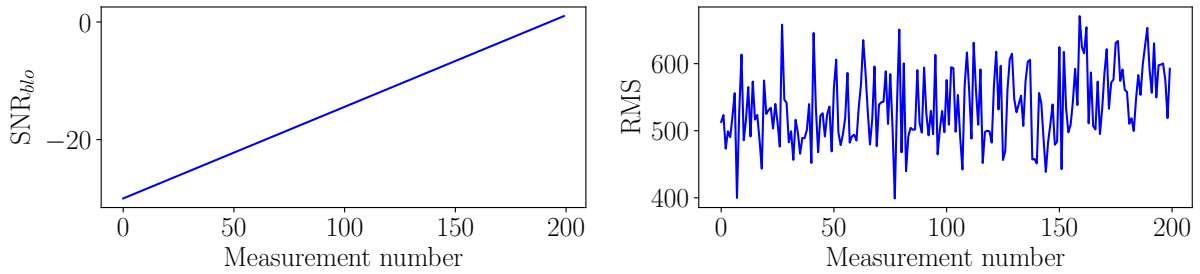


Figure B.20: The signal-to-noise ratio and the Root-Mean-Square (RMS) of the damaged bearing component are presented over measurement number. The signal-to-noise ratio is calculated with  $10 \log_{10}(E_b/E_n)$  where  $E_b$  is the energy of the bearing component and  $E_n$  is the energy of the noise component.

experiment. The kurtosis performs better than the RMS for both cases, but it contains much more noise than the condition indicators obtained with the proposed methodology. The L2/L1 ratio of the SES does not perform well on the considered dataset. Hence, it is clear that the proposed method performs very well in highlighting that the gearbox is damaged and that its health is deteriorating over measurement number.

## Acknowledgements

S. Schmidt gratefully acknowledges the Eskom Power Plant Engineering Institute (EPPEI) for their support in the execution of this research.

## References

- [1] J. Antoni, Cyclostationarity by examples, *Mechanical Systems and Signal Processing* 23 (4) (2009) 987–1036.
- [2] V. Girondin, K. M. Pekpe, H. Morel, J.-P. Cassar, Bearings fault detection in helicopters using frequency readjustment and cyclostationary analysis, *Mechanical Systems and Signal Processing* 38 (2) (2013) 499–514.
- [3] R. B. Randall, J. Antoni, S. Chobsaard, The relationship between spectral correlation and envelope analysis in the diagnostics of bearing faults and other cyclostationary machine signals, *Mechanical Systems and Signal Processing* 15 (5) (2001) 945–962.

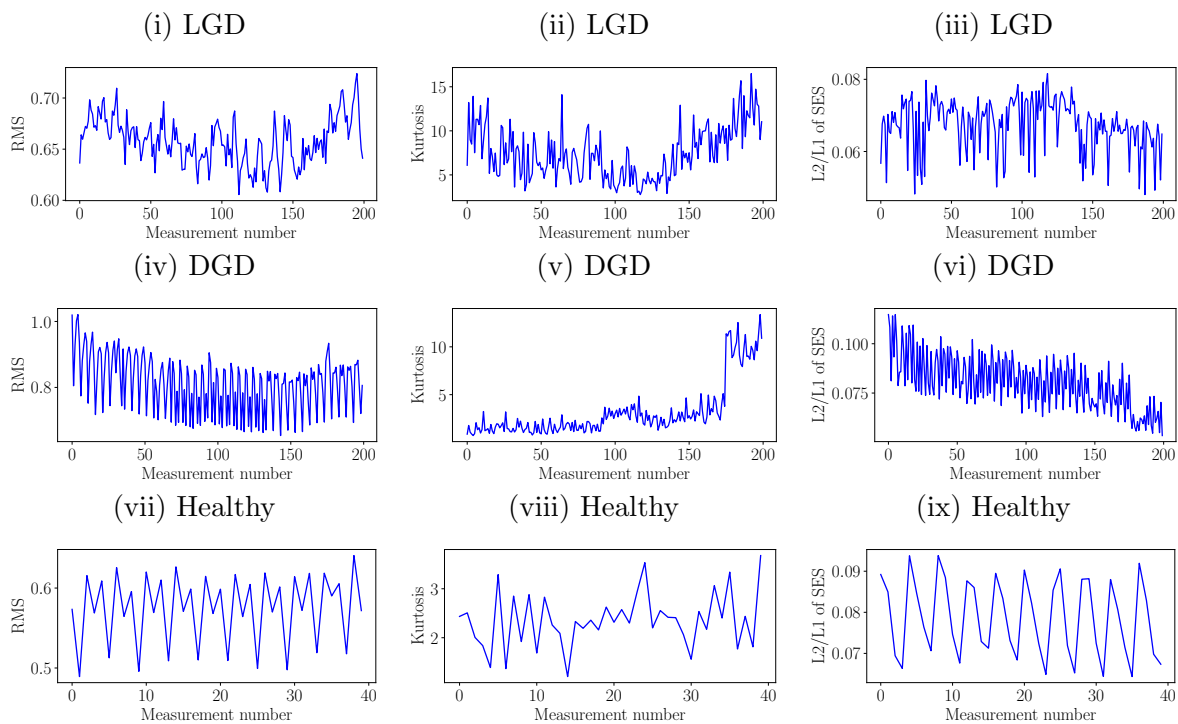


Figure C.21: Three blind metrics are calculated for different experimental signals considered in this work. Abbreviations: Localised Gear Damage (LGD) discussed in Section 4.2; Distributed Gear Damage (DGD) discussed in Section 4.3.

- [4] D. Abboud, J. Antoni, S. Sieg-Zieba, M. Eltabach, Envelope analysis of rotating machine vibrations in variable speed conditions: A comprehensive treatment, *Mechanical Systems and Signal Processing* 84 (2017) 200–226.
- [5] J. Urbanek, T. Barszcz, R. Zimroz, J. Antoni, Application of averaged instantaneous power spectrum for diagnostics of machinery operating under non-stationary operational conditions, *Measurement* 45 (7) (2012) 1782–1791.
- [6] N. Baydar, A. Ball, Detection of gear deterioration under varying load conditions by using the instantaneous power spectrum, *Mechanical Systems and Signal Processing* 14 (6) (2000) 907–921.
- [7] J. Antoni, Cyclic spectral analysis in practice, *Mechanical Systems and Signal Processing* 21 (2007) 597–630.

- 1  
2  
3 [8] J. Antoni, Cyclic spectral analysis of rolling-element bearing signals: Facts and fic-  
4 tions, *Journal of Sound and Vibration* 304 (3-5) (2007) 497–529.  
5  
6  
7  
8 [9] R. Zimroz, W. Bartelmus, T. Barszcz, J. Urbanek, Diagnostics of bearings in pres-  
9 ence of strong operating conditions non-stationarity - A procedure of load-dependent  
10 features processing with application to wind turbine bearings, *Mechanical Systems*  
11 *and Signal Processing* 46 (1) (2014) 16–27.  
12  
13  
14  
15  
16  
17 [10] D. Abboud, S. Baudin, J. Antoni, D. Rémond, M. Eltabach, O. Sauvage, The spectral  
18 analysis of cyclo-non-stationary signals, *Mechanical Systems and Signal Processing*  
19 75 (2016) 280–300.  
20  
21  
22  
23  
24 [11] J. Antoni, G. Xin, N. Hamzaoui, Fast computation of the spectral correlation, *Me-*  
25 *chanical Systems and Signal Processing* 92 (2017) 248–277.  
26  
27  
28  
29 [12] A. Mauricio, J. Qi, W. A. Smith, M. Sarazin, R. B. Randall, K. Janssens, K. Gryllias,  
30 Bearing diagnostics under strong electromagnetic interference based on integrated  
31 spectral coherence, *Mechanical Systems and Signal Processing* 140 (2020) 106673.  
32  
33  
34  
35  
36 [13] D. Wang, X. Zhao, L.-L. Kou, Y. Qin, Y. Zhao, K.-L. Tsui, A simple and fast guideline  
37 for generating enhanced/squared envelope spectra from spectral coherence for bearing  
38 fault diagnosis, *Mechanical Systems and Signal Processing* 122 (2019) 754–768.  
39  
40  
41  
42 [14] S. Schmidt, P. S. Heyns, K. C. Gryllias, A methodology using the spectral coherence  
43 and healthy historical data to perform gearbox fault diagnosis under varying operating  
44 conditions, *Applied Acoustics* 158 (2020) 107038.  
45  
46  
47  
48  
49  
50 [15] F. Jia, Y. Lei, J. Lin, X. Zhou, N. Lu, Deep neural networks: A promising tool  
51 for fault characteristic mining and intelligent diagnosis of rotating machinery with  
52 massive data, *Mechanical Systems and Signal Processing* 72-73 (2016) 303–315.  
53  
54  
55  
56  
57  
58 [16] Z. Chen, A. Mauricio, W. Li, K. Gryllias, A deep learning method for bearing fault  
59  
60  
61  
62  
63  
64  
65

- 1  
2  
3 diagnosis based on cyclic spectral coherence and convolutional neural networks, *Mechanical Systems and Signal Processing* 140 (2020) 106683.  
4  
5  
6  
7  
8 [17] S. Schmidt, P. S. Heyns, An open set recognition methodology utilising discrepancy  
9 analysis for gear diagnostics under varying operating conditions, *Mechanical Systems  
10 and Signal Processing* 119 (2019) 1–22.  
11  
12  
13  
14 [18] Q. Leclère, H. André, J. Antoni, A multi-order probabilistic approach for Instanta-  
15 neous Angular Speed tracking debriefing of the CMMNO'14 diagnosis contest, *Mechanical Systems and Signal Processing* 81 (2016) 375–386.  
16  
17  
18  
19  
20 [19] S. Lu, R. Yan, Y. Liu, Q. Wang, Tacholless speed estimation in order tracking: A  
21 review with application to rotating machine fault diagnosis, *IEEE Transactions on  
22 Instrumentation and Measurement* 68 (7) (2019) 2315–2332.  
23  
24  
25  
26  
27 [20] P. Borghesani, J. Antoni, A faster algorithm for the calculation of the fast spectral  
28 correlation, *Mechanical Systems and Signal Processing* 111 (2018) 113–118.  
29  
30  
31  
32  
33 [21] R. B. Randall, J. Antoni, Rolling element bearing diagnosticsa tutorial, *Mechanical  
34 systems and signal processing* 25 (2) (2011) 485–520.  
35  
36  
37  
38  
39 [22] W. A. Smith, P. Borghesani, Q. Ni, K. Wang, Z. Peng, Optimal demodulation-band  
40 selection for envelope-based diagnostics: A comparative study of traditional and novel  
41 tools, *Mechanical Systems and Signal Processing* 134 (2019) 106303.  
42  
43  
44  
45  
46 [23] A. Mauricio, W. A. Smith, R. B. Randall, J. Antoni, K. Gryllias, Improved envelope  
47 spectrum via feature optimisation-gram (iesfogram): A novel tool for rolling element  
48 bearing diagnostics under non-stationary operating conditions, *Mechanical Systems  
49 and Signal Processing* 144 (2020) 106891.  
50  
51  
52  
53  
54 [24] D. Wang, Spectral  $l_2/l_1$  norm: A new perspective for spectral kurtosis for character-  
55 izing non-stationary signals, *Mechanical Systems and Signal Processing* 104 (2018)  
56 290–293.  
57  
58  
59  
60  
61  
62  
63  
64  
65

1  
2  
3  
4  
5  
6  
7  
8  
9  
10  
11  
12  
13  
14  
15  
16  
17  
18  
19  
20  
21  
22  
23  
24  
25  
26  
27  
28  
29  
30  
31  
32  
33  
34  
35  
36  
37  
38  
39  
40  
41  
42  
43  
44  
45  
46  
47  
48  
49  
50  
51  
52  
53  
54  
55  
56  
57  
58  
59  
60  
61  
62  
63  
64  
65

[25] J. Antoni, The infogram: Entropic evidence of the signature of repetitive transients, *Mechanical Systems and Signal Processing* 74 (2016) 73–94.

[26] Y. Lin, L. Tu, H. Liu, W. Li, Fault analysis of wind turbines in China, *Renewable and Sustainable Energy Reviews* 55 (2016) 482–490.

# The anomalous and smoothed anomalous envelope spectra for rotating machine fault diagnosis

Stephan Schmidt<sup>a,\*</sup>, Konstantinos C. Gryllias<sup>b,c</sup>

<sup>a</sup>*Centre for Asset Integrity Management, Department of Mechanical and Aeronautical Engineering, University of Pretoria, Pretoria, South Africa*

<sup>b</sup>*Department of Mechanical Engineering, KU Leuven, Celestijnenlaan 300, 3001 Heverlee, Belgium*

<sup>c</sup>*Dynamics of Mechanical and Mechatronic Systems, Flanders Make, Belgium*

---

## Abstract

The order-frequency spectral coherence and its integrated spectra (e.g. improved envelope spectrum, squared envelope spectrum) are some of the most powerful methods for performing fault diagnosis under time-varying operating conditions. However, it may require much work to interrogate the order-frequency spectral coherence for symptoms of damage. Hence, in this work we propose a methodology that combines the order-frequency spectral coherence with historical data that were acquired from a healthy machine to obtain an anomalous envelope spectrum, which is further processed for fault diagnosis. This anomalous envelope spectrum is further processed with a smoothing operation to not only perform automatic fault detection, but it is also possible to identify the damaged component if the kinematics of the gearbox are known. The proposed method is investigated on one numerical gearbox dataset and three experimental datasets, where its potential for performing automatic fault detection under time-varying operating conditions is highlighted.

*Keywords:*

Anomalous envelope spectrum, Cyclostationary analysis, Novelty detection, Blind fault detection, Time-varying operating conditions

---

\*Corresponding author.

*Email address:* `stephan.schmidt@up.ac.za` (Stephan Schmidt)

## 1. Introduction

The vibration signals acquired from rotating machines are usually generated by periodic phenomena (e.g. gear mesh interactions, impacts due to bearing damage) [1]. As a result, the statistics of the signal are periodic in the angle domain and therefore the measured vibration signals can be described by the theory of cyclostationarity [1, 2]. This makes cyclostationary analysis techniques such as the squared envelope spectrum [3, 4], the instantaneous power spectrum [5, 6], the spectral correlation [7, 8] and the spectral coherence [7, 8] very powerful techniques for interrogating the vibration signals for symptoms of damage.

However, rotating machines such as wind turbines operate inherently under time-varying operating conditions [5, 9], which impedes the application of the conventional time- or angle-based cyclostationary techniques [10]. This is attributed to the fact that even though the instantaneous power of the bearing damage component is periodic in the angle domain, the carrier of the signal is described by the dynamic properties of the structure, which are time-invariant [10]. Hence, neither the time nor angle domain representations are suited to describe these signals, and the signals should rather be described using angle-time cyclostationary theory [10]. Hence, the angle-frequency instantaneous power spectrum [5], the order-frequency spectral correlation [10] and Order-Frequency Spectral Coherence (OFSCoh) [10] should be used for analysing the time-invariant second-order components of vibration signals that were acquired under time-varying speed conditions.

The OFSCoh is currently one of the most powerful techniques for performing bearing diagnostics under time-varying operating conditions [10]. It is a bivariate representation of the cyclic orders of the angle-periodic modulation components and the spectral frequencies of their time-invariant carriers [10]. However, the two-dimensional representation can be difficult to interrogate when incipient damage is present and therefore the integrated spectral coherence is very useful for fault diagnosis [8, 11–13].

However, applying state-of-the-art signal analysis techniques can require much work to implement and much manual effort to investigate for symptoms of damage. In some

1  
2  
3 cases the fault order of the component-of-interest needs to be specified a priori before  
4  
5 the method can be applied e.g., [2, 12, 14]. This means that the techniques could be  
6  
7 difficult to scale when many machines need to be monitored for damage. This has been  
8  
9 one of the main motivations of developing deep learning fault diagnosis methods [15]; the  
10  
11 methods make it possible to automatically determine the condition of the machine from  
12  
13 the raw or processed vibration signals. Chen et al. [16] combined the spectral coherence  
14  
15 and convolutional neural networks for automatic fault classification. However, many deep  
16  
17 learning methods require much historical fault data to be available and the classification  
18  
19 problem is actually an open set recognition problem (i.e. only historical fault data of  
20  
21 some of the damage modes may be available), which could make it difficult to apply the  
22  
23 supervised learning techniques in practice [17].  
24  
25

26 In Ref. [14], a methodology is proposed to combine the OFSCoh with healthy histor-  
27  
28 ical data. This is performed by firstly identifying the damage modes in the system and  
29  
30 targeting their specific cyclic orders in the OFSCoh. Subsequently, a data-driven model  
31  
32 was developed of the healthy behaviour of the features extracted from the targeted compo-  
33  
34 nents, which was then used to automatically infer the health of the targeted components.  
35  
36 However, if a complex drive train is under consideration, there may be many cyclic orders  
37  
38 that need to be targeted to properly monitor the machine. It is also possible that the  
39  
40 harmonics of the cyclic orders of different components can overlap, which may lead to  
41  
42 ambiguous behaviour when performing inference.  
43  
44

45 Hence, in this work we propose a blind methodology that can be used for performing  
46  
47 fault diagnosis under time-varying operating conditions. The outcome of this methodology  
48  
49 is the Anomalous Envelope Spectrum (AES) and the smoothed AES (sAES), which are  
50  
51 calculated by combining the OFSCoh and historical data from a healthy machine. The  
52  
53 AES is a powerful representation that can be used to detect faults and it can also help  
54  
55 to identify which components are damaged. It has the additional benefit, compared to  
56  
57 Ref. [14] for example, that it does not require the components-of-interest to be known  
58  
59 nor specified before applying the methodology, i.e. it is blind. It is only desirable to know  
60  
61  
62  
63  
64  
65



1  
2  
3 the kinematics of the gearbox if the AES is interrogated to determine which machine  
4  
5 component is damaged.  
6

7 In summary, the contributions of this paper are the following:  
8

- 9
- 10 • A new representation, the Anomalous Envelope Spectrum (AES), is proposed which  
11 can be processed to perform fault diagnosis under time-varying operating conditions.  
12 We propose using a smoothing operation between consecutive OFSCohs before the  
13 AES is calculated. This processed AES is referred to as the smoothed AES (sAES)  
14 in this work.  
15
  - 16 • This method is simple to implement and scalable for monitoring many machines.  
17 This is because historical data are used to supplement the OFSCoh for fault detection  
18 and identification under time-varying operating conditions, i.e. it is not necessary  
19 to manually interrogate the signals.  
20

21 The layout of the paper is as follows: In Section 2, an overview of the proposed  
22 method is given, whereafter the method is applied on numerical gearbox data in Section  
23 3 and on three experimental gearbox datasets in Section 4. **In Section 5, additional**  
24 **analyses are performed to quantify the calculation time of the proposed method and to**  
25 **highlight the influence of the historical data on the proposed method.** Finally, the paper  
26 is concluded in Section 6. Appendix A contains additional information pertaining to the  
27 threshold selection discussed in Section 2; Appendix B contains additional information of  
28 the numerical gearbox model presented in Section 3; and Appendix C contains additional  
29 results obtained on the experimental data discussed in Section 4.  
30

## 31 **2. Proposed methodology**

32

33 We desire to develop a vibration-based condition monitoring methodology that enables  
34 us to determine the condition of the machine at measurement  $i$ , without requiring the  
35 cyclic orders of interest to be specified beforehand, i.e. the methodology is blind. This  
36 methodology is developed under the following assumptions:  
37  
38  
39  
40  
41  
42  
43  
44  
45  
46  
47  
48  
49  
50  
51  
52  
53  
54  
55  
56  
57  
58  
59  
60  
61  
62  
63  
64  
65

- There are much historical data available that describe the behaviour of the machine in a reference condition, whereafter the machine is monitored for damage.
- An accurate estimate of the rotational speed is available at each measurement, with the rotational speed at measurement  $i$  denoted by  $\omega^{(i)}(t)$ . If the speed cannot be measured, it is possible to use a tachless speed estimation method [18, 19] before applying this methodology.
- Regular measurements are taken during the condition monitoring process. The vibration signal acquired at measurement  $i$  is denoted by  $x^{(i)}(t)$  and its corresponding sampling frequency is  $f_s$ .

### 2.1. Preliminary theory

The Order-Frequency Spectral Coherence (OFSCoh) can highlight weak damage components in the signal and therefore enables incipient damage to be detected [10, 11]. The OFSCoh of the vibration measurement acquired at time step  $i$  [10]

$$\gamma^{(i)}(\alpha, f) = \frac{S_{xx}^{(i)}(\alpha, f)}{\left| S_x^{(i)}(0, f) \cdot S_{x_\alpha}^{(i)}(0, f) \right|^{1/2}}, \quad (1)$$

is calculated with the order-frequency spectral correlation  $S_{xx}^{(i)}(\alpha, f)$ , the power spectral density of the vibration signal  $x^{(i)}(t)$  denoted by  $S_x^{(i)}(0, f)$  and the power spectral density of  $x_\alpha^{(i)}(t) = x^{(i)}(t) \cdot e^{-j\alpha\theta^{(i)}(t)} \cdot \omega^{(i)}(t)$  denoted by  $S_{x_\alpha}^{(i)}(0, f)$  [10]. The imaginary unit is denoted by  $j = \sqrt{-1}$ . In Equation (1),  $\alpha$  denotes the cyclic order variable and  $f$  denotes the spectral frequency variable. The order-frequency spectral correlation is calculated with [10]

$$S_{xx}^{(i)}(\alpha, f) = \lim_{W \rightarrow \infty} \frac{1}{\Phi(W)} \mathbb{E} \left\{ \mathcal{F}_W(x^{(i)}(t))^* \cdot \mathcal{F}_W \left( x^{(i)}(t) \cdot e^{-j\alpha\theta^{(i)}(t)} \cdot \omega^{(i)}(t) \right) \right\}, \quad (2)$$

where  $\mathcal{F}_W(\cdot)$  is the Fourier transform over a time length of  $W$ ,  $x^{(i)}(t)$  is the measurement taken at time step  $i$ ,  $\omega^{(i)}(t)$  is the corresponding instantaneous rotational speed of a shaft

1  
2  
3 and  $\theta^{(i)}(t)$  is the corresponding instantaneous phase of the shaft. The cumulative phase of  
4  
5 the shaft after a time duration of  $W$  is denoted  $\Phi(W)$ . The reason why the measurement  
6  
7 index  $i$  is emphasised in all of the terms, is because this is important for the calculation of  
8  
9 the processed AES and it ensures that a consistent notation is used. The order-frequency  
10  
11 spectral correlation is estimated with the Welch-based estimator proposed in Ref. [10], due  
12  
13 to its good bias and variance properties. However, much faster estimators of the spectral  
14  
15 correlation can be used if desired [11, 20].

16  
17 The integrated spectral coherence is very useful for gearbox diagnostics, due to the  
18  
19 fact that it is simpler to interrogate for damage than the bivariate OFSCoh [12, 13]. The  
20  
21 Squared Envelope Spectrum is the most popular signal analysis technique for performing  
22  
23 bearing fault diagnosis [4] and can be estimated from the OFSCoh with [11, 13, 21]

$$24 \quad \text{SES}^{(i)}(\alpha) = \left| \int_0^{f_s/2} \gamma^{(i)}(\alpha, f) df \right|, \quad (3)$$

25  
26 for the  $i$ th signal, while the enhanced envelope spectrum can be estimated with

$$27 \quad \text{EES}^{(i)}(\alpha) = \int_0^{f_s/2} |\gamma^{(i)}(\alpha, f)|^2 df. \quad (4)$$

28  
29 The sampling frequency of the signal is denoted by  $f_s$ . It was shown in Ref. [11] that in  
30  
31 general the EES is better suited for incipient fault detection than the SES. Hence, it is  
32  
33 possible to estimate the SES and the EES with Equations (3) and (4) without performing  
34  
35 bandpass filtering on the raw vibration signal.

36  
37 It is possible to improve the signal-to-noise ratio of the damaged components in the  
38  
39 integrated spectrum by limiting the integration band of the SES and the EES to a band  
40  
41  $[f_l, f_h]$ . This is because the impulses generated by damaged components excite resonances  
42  
43 in the system, which means that the fault information manifests in narrow frequency bands  
44  
45 [22]. The integration of the OFSCoh over the band  $[f_l, f_h]$  is used to define the Improved  
46  
47

Envelope Spectrum (IES) [11],

$$\text{IES}^{(i)}(\alpha; f_l, f_h) = \int_{f_l}^{f_h} |\gamma^{(i)}(\alpha, f)|^2 df, \quad (5)$$

where  $0 < f_l < f_h$  and  $f_h < f_s/2$ . Therefore, if the integration band  $[f_l, f_h]$  is carefully selected, the IES can improve the signal-to-noise ratio of the fault information. However, selecting the appropriate frequency band automatically can be difficult to perform, especially if the fault information is weak. This has resulted in the development of the IESFOgram, which aims to detect the frequency band that is optimal for detecting specific targeted signal components [23]. Even though the IESFOgram performs very well in identifying the optimal integration band, it requires the targeted cyclic orders to be specified a priori. This can be difficult when complicated drive-trains with many fault orders need to be monitored or when the fault orders are not known.

The proposed methodology was developed to allow us to automatically identify the frequency bands that have important information and then to use this to obtain an intuitive representation for fault diagnosis. The Anomalous Envelope Spectrum (AES) is presented in the next section.

## 2.2. Anomalous Envelope Spectrum (AES)

The AES is derived from the Generalised Integrated Spectrum (GIS) in this work. The GIS of the  $i$ th vibration measurement is obtained from the integrated spectrum of the OFSCoh by including a general weighting function  $\mathcal{G}(\alpha, f)$

$$\text{GIS}^{(i)}(\alpha) = \int_0^{f_s/2} |\gamma^{(i)}(\alpha, f)|^2 \cdot \mathcal{G}(\alpha, f) df, \quad (6)$$

where the weighting function  $0 \leq \mathcal{G}(\alpha, f) \leq 1$ . This GIS has the following properties:

- The EES is obtained by setting  $\mathcal{G}(\alpha, f) = 1 \forall f \in [0, f_s/2]$ , i.e. then  $\text{GIS}^{(i)}(\alpha) = \text{EES}^{(i)}(\alpha)$ .

- The IES is obtained by setting  $\mathcal{G}(\alpha, f) = 1 \forall f \in [f_l, f_h]$  and  $\mathcal{G}(\alpha, f) = 0 \forall f \notin [f_l, f_h]$ , i.e. then  $\text{GIS}^{(i)}(\alpha) = \text{IES}^{(i)}(\alpha; f_l, f_h)$ .

Since it is assumed that healthy historical data are available, it is possible to construct a function  $G(\alpha, f)$  to automatically highlight regions in the OFSCoh that have non-healthy (i.e. anomalous) behaviour. This anomaly function  $G(\alpha, f)$  indicates whether healthy ( $G(\alpha, f) = 0$ ) or anomalous ( $G(\alpha, f) = 1$ ) behaviour is seen at a cyclic order  $\alpha$  and a spectral frequency  $f$  in  $|\gamma^{(i)}(\alpha, f)|^2$ . If we use this anomaly function  $G(\alpha, f)$  in the GIS, the Anomalous Envelope Spectrum (AES)

$$\text{AES}^{(i)}(\alpha) = \int_0^{f_s/2} |\gamma^{(i)}(\alpha, f)|^2 \cdot G(\alpha, f) df, \quad (7)$$

is obtained. The AES is used to identify components that are anomalous (e.g. attributed to machine damage or spurious noise). Hence, as opposed to selecting or estimating the optimal  $f_l$  and  $f_h$  to determine the IES with the GIS, only the information from anomalous frequency bands are retained in the AES.

### 2.3. Estimation of the AES

The OFSCohs associated with the  $N_h$  measurements from a healthy machine, denoted by  $\{\gamma_h^{(i)}(\alpha, f)\}_{i \in \mathbb{Z}, 0 \leq i \leq N_h - 1}$ , are used to calculate a threshold  $\tau(\alpha, f)$ . This threshold is used to automatically determine whether a specific combination of cyclic orders and spectral frequencies of the  $i$ th measurement contain anomalous information  $|\gamma^{(i)}(\alpha, f)|^2 > \tau(\alpha, f)$  or not  $|\gamma^{(i)}(\alpha, f)|^2 \leq \tau(\alpha, f)$ . This is used to define the anomaly function  $G$  for the measurement at time step  $i$  as follows:

$$G^{(i)}(\alpha, f) = \begin{cases} 1 & \text{if } |\gamma^{(i)}(\alpha, f)|^2 > \tau(\alpha, f) \\ 0 & \text{if } |\gamma^{(i)}(\alpha, f)|^2 \leq \tau(\alpha, f). \end{cases} \quad (8)$$

It is possible to use kernel density estimators to detect anomalous behaviour with the spectral coherence as investigated in Ref. [14], however, this can be computationally

intensive to use and it is required to find the optimal hyperparameters for each combination of  $\alpha$  and  $f$ . If it is assumed that the data are Gaussian, the threshold can be defined by:

$$\tau(\alpha, f) = \mu_\gamma(\alpha, f) + \kappa \cdot \sigma_\gamma(\alpha, f), \quad (9)$$

where  $\kappa$  is a factor,  $\mu_\gamma(\alpha, f)$  is the mean and  $\sigma_\gamma(\alpha, f)$  is the standard deviation of the healthy spectral coherences. However, the sampling distribution of the spectral coherence is not expected to be Gaussian. In Ref. [7], it was shown that the distribution of the spectral coherence is asymptotically chi-square distributed. Using the empirical distribution of the data to set the threshold is another approach that can be used. For example, the inter-percentile range can be used to obtain a threshold with

$$\tau(\alpha, f) = \kappa \cdot (p_\xi(\alpha, f) - p_{100-\xi}(\alpha, f)) + p_{100-\xi}(\alpha, f), \quad (10)$$

where  $p_\xi(\alpha, f)$  is the  $\xi$ th percentile of the set of healthy spectral coherences, denoted by  $\{\gamma_h^{(i)}(\alpha, f)\}$ , at a specific cyclic order  $\alpha$  and spectral frequency  $f$ . A special case of this range is the interquartile range where  $\xi = 75$ . If  $\kappa = 1$ , it means that the  $\xi$ th percentile is used for detecting outliers, which could result in false alarms. In addition to this, the threshold in Equation (10) is estimated from limited healthy measurements and is therefore a random variable. Hence, it is therefore suggested that  $\kappa > 1$ . In a practical situation, it would be better to use different  $\kappa$ s to obtain a range of thresholds for decision making, e.g. one threshold can act as a warning and another threshold can automatically stop the machine. The interpretation and use of the threshold would depend on the machine and its application (e.g. implications of a sudden failure).

The OFSCoh is estimated from a finite length signal and since the OFSCoh is sensitive to weak components in the signal, it could contain spurious noise. This would result in the anomaly function  $G^{(i)}(\alpha, f)$  to indicate anomalous behaviour, i.e.  $G^{(i)}(\alpha, f) = 1$ , for healthy cyclic orders and spectral frequencies. The robustness of the AES can be increased

by utilising the information from consecutive measurements to obtain the smoothed AES (sAES), which is a more robust representation of the condition of the gearbox under consideration. The smoothed AES (sAES) is calculated with

$$\text{sAES}^{(i)}(\alpha) = \int_0^{f_s/2} \mathcal{P} \{ |\gamma^{(m)}(\alpha, f)|^2 \cdot G^{(m)}(\alpha, f) \}_{m \in \mathbb{Z}, i - N_s \leq m \leq i} df, \quad (11)$$

where  $N_s$  is the number of consecutive measurements that is used for processing the weighted spectral coherences  $|\gamma^{(m)}(\alpha, f)|^2 \cdot G^{(m)}(\alpha, f)$ . We refer to this AES as the smoothed AES so that it is not confused with the raw AES obtained with Equation (7). The smoothing function  $\mathcal{P}$  can for example be the median or the mean. If the mean is used, the integrated spectrum of the moving averaged OFSCoh, i.e. the average of  $|\gamma^{(m)}(\alpha, f)|^2 \cdot G^{(m)}(\alpha, f)$  is calculated over measurement index  $m$ . The sAES can subsequently be used for automatic fault detection by searching for cyclic orders where  $\text{sAES}^{(i)}(\alpha) > 0$  and if the kinematics of the drive train are known, it would also be possible to identify the damaged component.

Lastly, the sAES can be used to obtain a simple Condition Indicator (CI) for time step  $i$  as follows:

$$\text{CI}_i = \frac{1}{\alpha_{max}} \int_0^{\alpha_{max}} \text{sAES}^{(i)}(\alpha) d\alpha, \quad (12)$$

with  $\text{CI}_i > 0$  indicates that anomalous behaviour is present, while  $\text{CI}_i = 0$  indicates that the spectral coherence of the measurement at time step  $i$  displays healthy behaviour. Since the smoothing operation removes the spurious anomalous components, the threshold can be set to  $\text{CI}_i = 0$  for detecting anomalous behaviour, which is used in the investigations of this paper. It is also possible to investigate other blind features such as the L2/L1 ratio [24] or the spectral negentropy [25] of the AES, but the optimisation of the condition indicator and the threshold selection is not considered in this work.

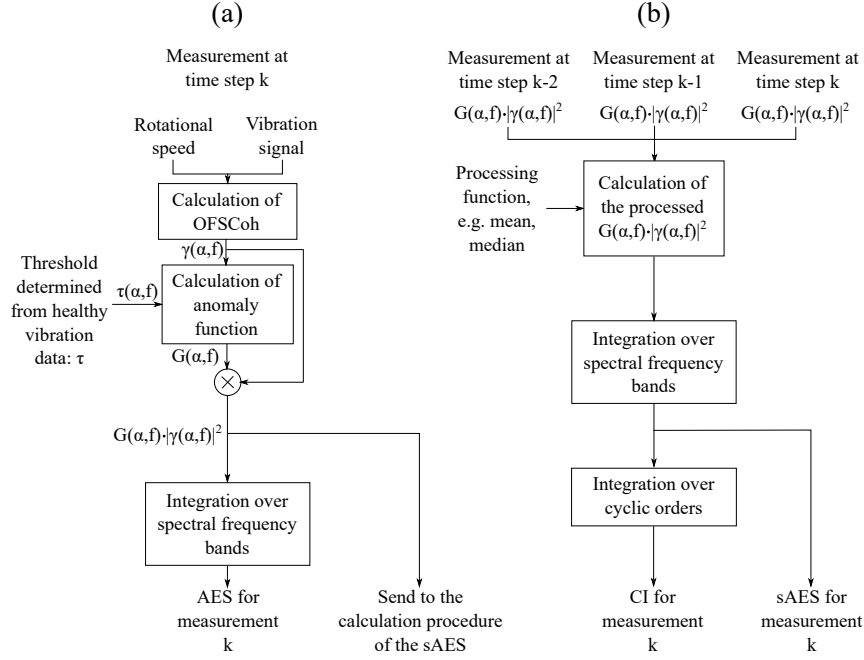


Figure 1: The calculation procedure of the Anomalous Envelope Spectrum (AES) for measurement  $k$  is shown in (a), while the calculation procedure of the smoothed AES (sAES) and its corresponding Condition Indicator (CI) are shown at time step  $k$  by using the information from the previous 3 time steps, i.e.  $N_s = 3$  in Equation (11).

#### 2.4. Summary

The calculation procedures of the AES and the sAES that were described in the previous sections are summarised in Figures 1(a) and 1(b) for time step  $k$ . The following parameters are used in all investigations:

- The median is used as the processing function  $\mathcal{P}$  in Equation (11). The median is much more robust to outliers than the mean and can therefore provide a more reliable estimate of the actual condition of the machine.
- The number of measurements used in calculating the sAES, i.e.  $N_s$  in Equation (11), is set to  $N_s = 10$ .
- The percentile  $\epsilon$  and the factor  $\kappa$  in Equation (10) are set to  $\epsilon = 95$  and  $\kappa = 4$ , respectively. The 95 percentile is used, because it is assumed that the healthy dataset does not contain much outliers and we desire to utilise the full distribution for detecting outliers in the damaged signal. We have found that  $\kappa = 4$  ensures that



1  
2  
3 the method is not too sensitive to outliers attributed to noise in the data and can  
4  
5 therefore result in less false alarms, while still performing very well in fault detection  
6  
7 and fault trending. The  $\kappa$  is further motivated in Section 4.2 and Appendix A.  
8  
9

10 This method is firstly investigated on numerical gearbox data in the next section, where-  
11  
12 after the method is investigated on three experimental gearbox datasets in Section 4.  
13  
14

### 15 16 **3. Numerical gearbox investigation** 17

18  
19 The phenomenological gearbox model presented in Ref. [4] is considered in this work  
20  
21 to simulate vibration data acquired from a gearbox operating under time-varying speed  
22  
23 conditions. The measured casing vibration signal of the gearbox in its reference condition  
24  
25

$$26 \quad x_c(t) = x_{gmc}(t) + x_{dgd}(t) + x_n(t), \quad (13)$$

27  
28  
29  
30 is decomposed in terms of three components, namely, a deterministic gear mesh component  
31  
32 denoted  $x_{gmc}(t)$ , a random gear component attributed to distributed gear damage denoted  
33  
34 by  $x_{dgd}(t)$  and a broadband noise component denoted by  $x_n(t)$ . Forty measurements  
35  
36 were taken from the gearbox in its reference condition, whereafter an additional signal  
37  
38 component due to outer race bearing damage is added to the casing vibration signal. The  
39  
40 new casing vibration signal  
41  
42

$$43 \quad x_c(t) = x_{gmc}(t) + x_b(t) + x_{dgd}(t) + x_n(t), \quad (14)$$

44  
45  
46  
47  
48 contains the additional bearing damage component denoted  $x_b(t)$ . More information re-  
49  
50 garding the signal components is given in Appendix B. Two-hundred measurements from  
51  
52 the damaged gearbox are investigated in this section, with the magnitude of the bear-  
53  
54 ing component increasing monotonically with the measurement number as discussed in  
55  
56 Appendix B and shown in Figure B.20.  
57  
58

59 The time-varying rotational speed profiles that were used to generate the vibration  
60  
61  
62  
63  
64  
65

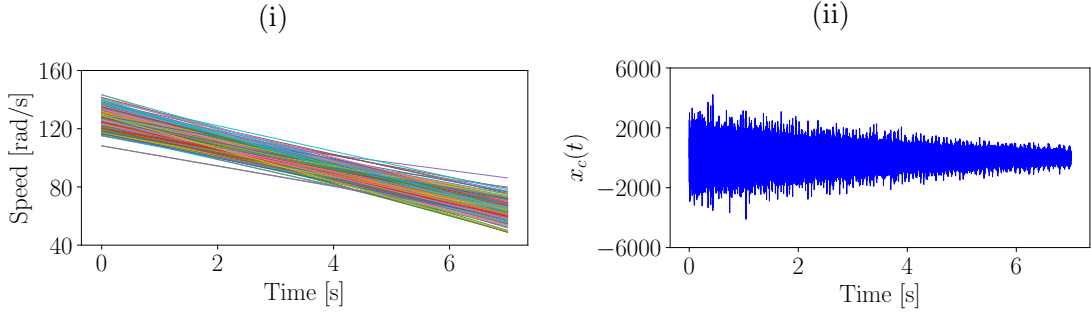


Figure 2: The rotational speeds that are under consideration in the phenomenological gearbox data as well as the vibration signal corresponding to the 110th measurement of the damaged gearbox.

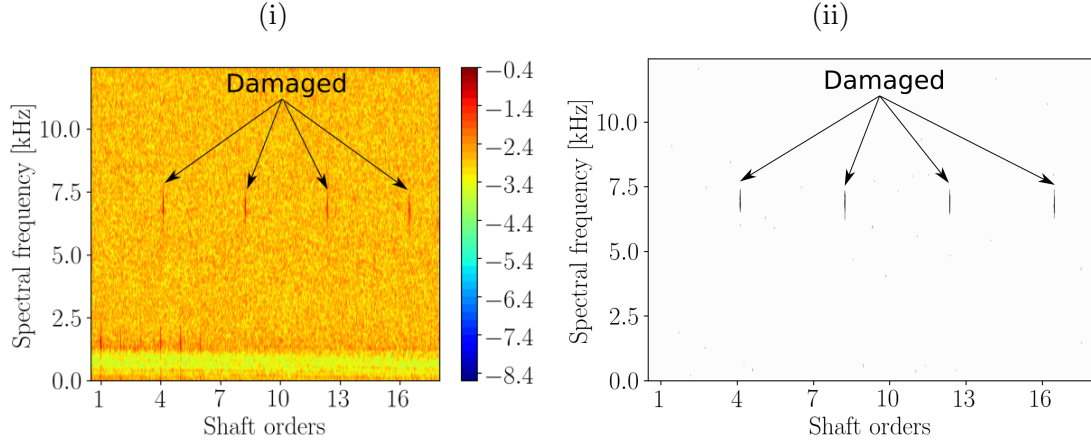


Figure 3: The OFSCoh of the vibration signal is presented in Figure 3(i) for the 110th measurement in the damaged dataset. The corresponding weighted OFSCoh is presented in Figure 3(ii).

data are presented in Figure 2(i). The casing vibration signal of the 110th measurement from the damaged gearbox (i.e. Equation (14)) shown in Figure 2(ii) is used to illustrate the different steps of the proposed method in this section.

The OFSCoh of the damaged gearbox is presented in Figure 3(i) for the measurement considered in Figure 2(ii). In Figure 3(i), the distributed gear damage component is clearly seen at a spectral frequency of 1.3 kHz and the components associated with the bearing damage are seen at 7 kHz. The methodology was applied on the 110th measurement of the considered dataset to obtain the resulting weighted OFSCoh, which is presented in Figure 3(ii). The weighted OFSCoh, calculated with  $G^{(i)}(\alpha, f) \cdot |\gamma^{(i)}(\alpha, f)|^2$ , only contains the bearing component at the spectral frequency of 7kHz, because the bearing damage

component is the only novel component in the signal. Hence, the weighted OFSCoh is able to enhance the novel components in the signal and attenuate the dominant components that were in the reference signal.

The integrated spectra, i.e. the EES, the AES and the sAES, are presented in Figure 4 for two measurements. No additional processing was performed before the EES and AES were calculated. The distributed gear damage component, with a cyclic order of 1.0 shaft orders, is dominant in the OFSCoh and therefore makes the weak bearing damage components more difficult to detect in the EES shown in Figure 4. Since both signals are random, they cannot be separated using techniques such as the generalised synchronous average [4]. In contrast to the EES, the bearing damage components are very prominent in the AES and the sAES, since the distributed gear damage components are removed in the weighted OFSCoh presented in Figure 3(ii). The sAES contains much less noise than the AES due to the additional processing that is performed.

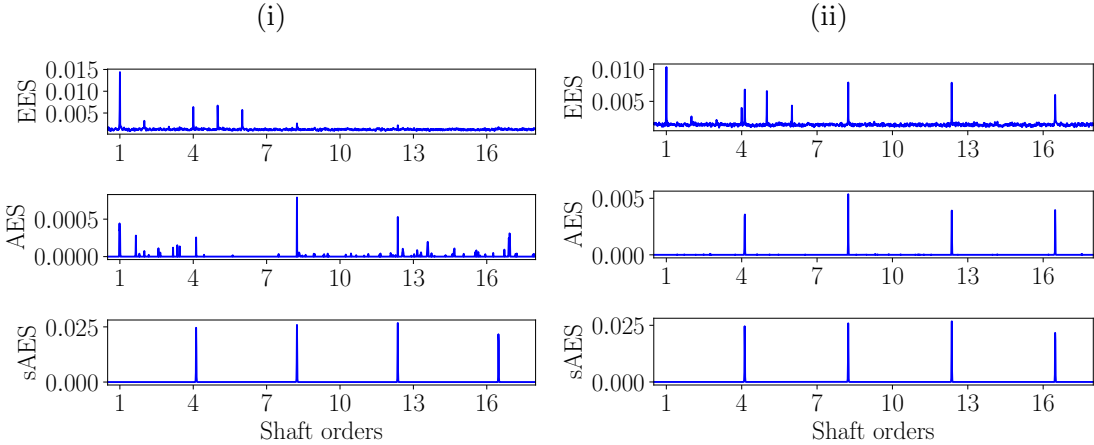


Figure 4: The integrated spectra are presented for two measurements in the damaged gearbox dataset. The integrated spectra of the 77th measurement and 110th measurement are presented in Figures 4(i) and 4(ii) respectively.

Since it is not only important to determine whether it is possible to detect bearing damage, but also whether changes in the condition can be detected, different magnitudes of bearing impulses are investigated. The magnitude of the bearing impulses were increased monotonically over the measurement number. Please refer to Figure B.20 for more infor-

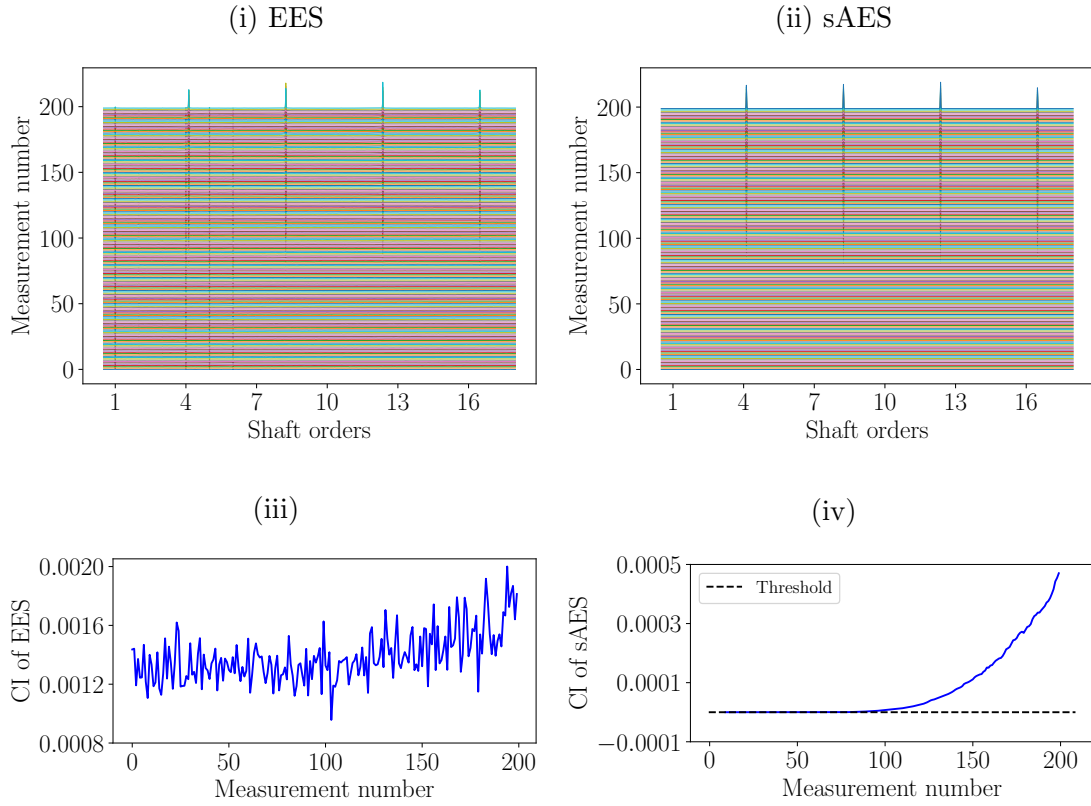


Figure 5: A waterfall plot of the EES and the sAES as well as their corresponding condition indicators are presented for the phenomenological gearbox model.

mation. The EES and the sAES of the different measurements under consideration are presented in Figures 5(i) and 5(ii), respectively. The exact signal-to-noise ratios of the bearing component for each measurement are included in Appendix B. The distributed gear damage and bearing damage components can be seen in the EES presented in Figure 5(i), while the sAES does not contain any signal components until the bearing damage component is detected. The bearing damage components at 4.12 shaft orders and its harmonics are clearly seen.

The mean of the integrated spectra are investigated as condition indicators for fault trending. The mean of the EES and the mean of the sAES as calculated with Equation (12) are presented in Figures 5(iii) and 5(iv) respectively. The condition indicator of the EES contains much noise which makes it difficult to observe the increase of the condition indicator due to the change in the magnitude of the bearing component. However, the CI

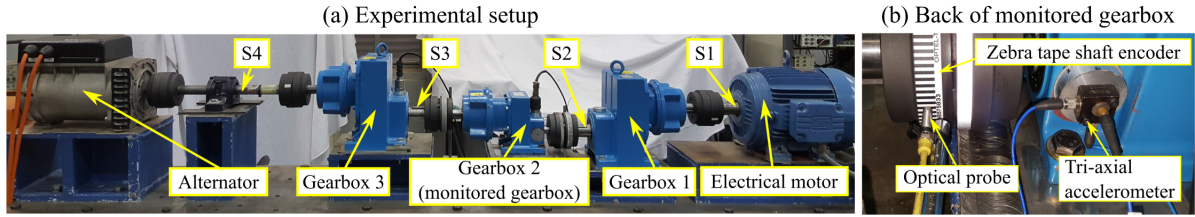


Figure 6: The experimental setup with the important components and parts highlighted.

of the sAES performs much better, due to the fact that it is not affected by the noise in the signal and provides a monotonic trend which is consistent with the magnitude of the bearing impulses that increases monotonically over the measurement number.

Hence, the proposed anomalous envelope spectrum and its related metrics are not only capable of detecting changes in the condition of the bearing, but it is also able to identify at which cyclic orders the damage manifests when inspecting the sAES. In the next section, the proposed method is investigated on experimental data.

#### 4. Experimental gearbox investigation

The proposed method is now investigated on experimental data that were acquired from a helical gearbox under time-varying operating conditions. In Section 4.1, an overview of the experimental setups and the measurement equipment is given, whereafter measurements taken from a gearbox with localised gear damage are investigated in Section 4.2 and measurements taken from a gearbox with distributed gear damage are investigated in Section 4.3. Finally, the method is investigated on healthy gearbox data in Section 4.4.

##### 4.1. Experimental setup

The data considered in this section were acquired from the experimental setup shown in Figure 6. The experimental setup consists of three helical gearboxes, an alternator and an electrical motor. The shafts between the different components are denoted by S1, S2, S3 and S4 respectively. The centre helical gearbox is monitored for damage with two accelerometers, namely, a single-axis accelerometer and a tri-axial accelerometer. The methodology is applied on the axial-component of the tri-axial accelerometer, which is

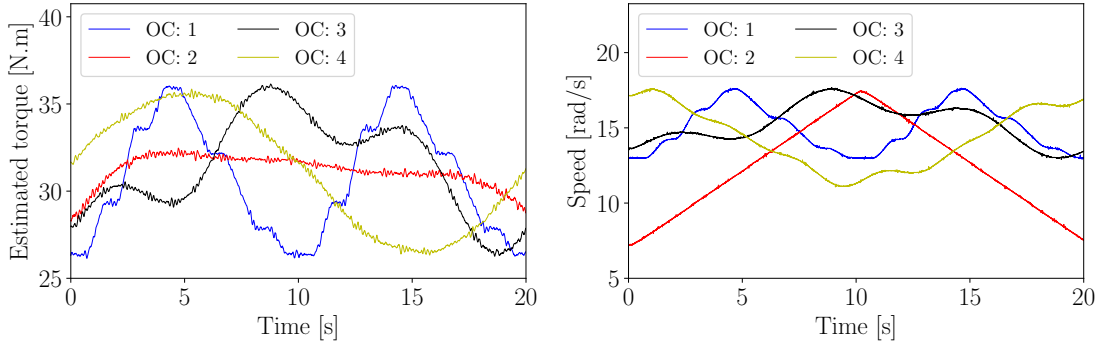


Figure 7: The operating conditions that were estimated at the input shaft of the gearbox, i.e.  $S_2$  in Figure 6.

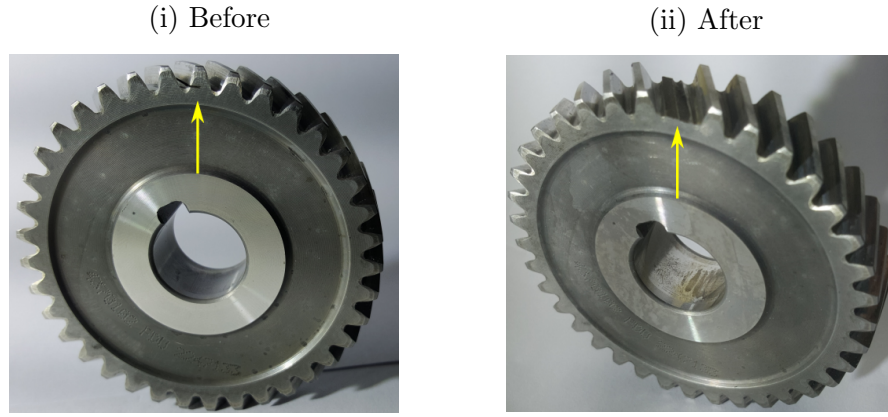
located on the bearing housing of the monitored gearbox as seen in Figure 6(b). The instantaneous speed of the input shaft of the gearbox (i.e.  $S_2$  in Figure 6) was measured with the optical probe and the zebra tape shaft encoder also shown in Figure 6(b). An OROS OR 35 data acquisition device was used with an accelerometer signal that was sampled at a rate of 25.6 kHz, while the optical probe was sampled at 51.2 kHz.

The electrical motor and the alternator were independently controlled to apply the time-varying operating conditions to the monitored gearbox as shown in Figure 7.

The monitored helical gearbox in Figure 6 consists of a gear and a pinion. The pinion was kept healthy for all measurements, while the gear was damaged as discussed in the next sections. Since the gear is connected to the reference shaft  $S_2$  in Figure 6, it rotates at 1.0 shaft order. This means that impacts from a damaged gear tooth would modulate the signal at 1.0 shaft order and would therefore be detected at 1.0 shaft order and its harmonics when interrogating the envelope spectrum. In Appendix C, the RMS, the kurtosis and the L2/L1-norm ratio of the SES are presented for the raw vibration signals considered in this work. This is to further highlight the benefits of using the proposed method.

#### 4.2. Localised gear damage experiment

Localised gear damage such as root cracks can severely affect the remaining useful life of gearboxes and is therefore very important to detect. An experiment was firstly performed with both gears of the monitored gearbox being healthy. Forty measurements, taken while



17  
18  
19  
20  
21

Figure 8: The gear with localised gear damage is presented. In Figure 8(i), the gear before the fatigue experiment is presented, while in Figure 8(ii) the gear after the fatigue experiment is presented. The seeded slot was 50% of the tooth thickness deep and had a height of 0.3 mm.

22  
23  
24  
25  
26  
27  
28  
29  
30  
31  
32  
33  
34  
35  
36  
37  
38  
39  
40  
41  
42

the gearbox was operating under operating condition 1 in Figure 7, are used to calculate the bivariate threshold function  $\tau(\alpha, f)$  with Equation (10). Thereafter, the gearbox was disassembled and the gear was damaged by seeding a small slot in the root of the gear tooth as shown in Figure 8(i). The helical gears have much larger contact ratios than spur gears and vibration signals contain impulsive components that make the gear damage shown in Figure 8(i) more difficult to detect. The monitored gearbox was reassembled with the damaged gear and tested for approximately 20 days under operating condition 1 before the damaged tooth failed as shown in Figure 8(ii). Two-hundred measurements, approximately evenly spaced over the testing period, are used to evaluate the effectiveness of this methodology.

43  
44  
45  
46  
47  
48  
49  
50  
51  
52  
53  
54  
55  
56  
57  
58  
59  
60  
61  
62  
63  
64  
65

However, this experiment does not represent the actual conditions that would be expected in a real application. If maintenance is performed on the system, the damaged components would be replaced with healthy components, which would make new measurements available for calculating the threshold  $\tau$ . In this experiment, we needed to replace the gear with a damaged gear to ensure that the gear would fail in a reasonable time. The implication of this is that there may be some differences between the experimental setup under consideration and the reference experimental setup which could also result in the measurements to have different statistical properties. Hence,  $\kappa$  in Equation (10) was made sufficiently large (i.e.  $\kappa = 4$ ) to ensure that false alarms are avoided.



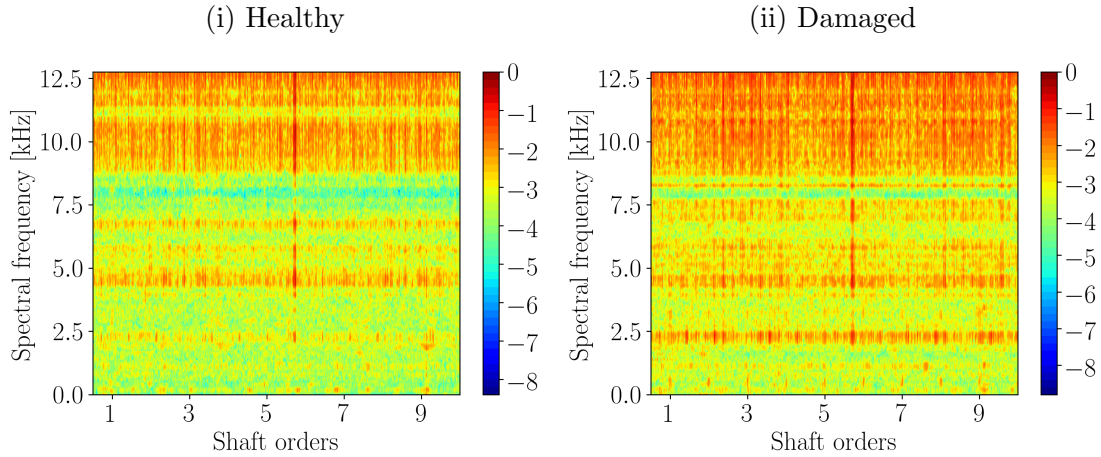


Figure 9: The logarithm of the mean OFSCoh of the healthy data and the logarithm of the OFSCoh from a damaged signal are presented in Figures 9(i) and 9(ii) on different colour scales.

The average spectral coherences of the healthy measurements are presented in Figure 9(i) to emphasise the motivation of using a bivariate threshold  $\tau(\alpha, f)$  in the method. If the threshold was set to a constant value for all cyclic orders and spectral frequencies, it may be too sensitive to noise at specific combinations of  $\alpha$  and  $f$ , while being insensitive to damage at other combinations of  $\alpha$  and  $f$ . The OFSCoh of one of the measurements from the damaged gearbox is presented in Figure 9(ii). The damaged components are located in a resonance band at approximately 500 Hz, but the OFSCoh is dominated by other phenomena which make the damage difficult to detect.

The corresponding weighted OFSCoh is presented in Figure 10(i). Since the impacts attributed to localised gear damage are the only new information in the signal, the weighted OFSCoh retains only the damaged information in the aforementioned frequency bands as seen in Figure 10(i). Since the damage only manifest in a very localised region of the OFSCoh, a zoomed view is included in Figure 10(i). Lastly, the different integrated OFSCoh of the measurement from the damaged gearbox are presented in Figure 10(ii). The EES only retains a strong component at 5.72 shaft orders, but the components attributed to the gear damage cannot be clearly seen. The AES and the sAES perform much better, because they are able to identify the damaged components in the signal, with the sAES containing a much clearer representation due to the additional processing that is



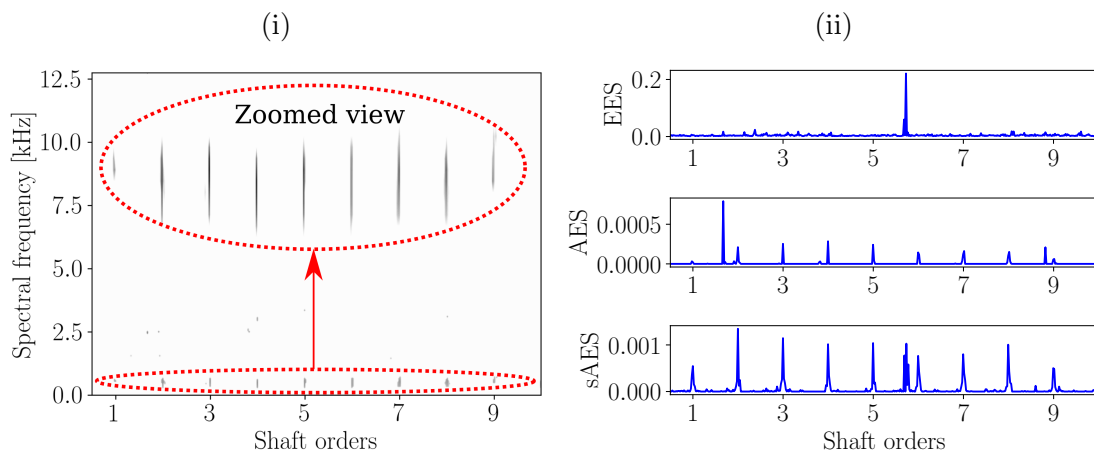


Figure 10: The weighted OFSCoh and corresponding integrated spectra are presented for the same signal considered in Figure 9(ii).

performed. Hence, it is clear that the proposed method is a very powerful representation for identifying frequency bands with novel information and using this not only for fault detection, but also for fault identification.

The EES and the sAES are presented over the measurement number in Figure 11. The EES contains the very strong component at 5.72 shaft orders for all measurements, while being unable to detect the damaged gear component. This dominant impulsive signal component is present in both the healthy and the damaged datasets, however, it impedes the detection of the damaged gear component. The signal component at 5.72 shaft orders is attributed to the movement of the floating shaft in the monitored gearbox that results in undesired contact between the bearing and the casing of the gearbox. The movement is exacerbated by the fact that the input shaft of the helical gearbox has strong axial excitations due to the axial forces of the helical gears.

In contrast, the sAES performs much better than the EES. In the sAES in Figure 11, the signal components associated with the damaged gear are very prominent in the spectrum, while it is also possible to see the degradation of the components over time as the condition of the gear worsens. Lastly, the Condition Indicator (CI) is calculated from the EES and the sAES and presented in Figure 12 over the measurement number. It is not possible to see the deterioration of the gear in the EES feature, because the signal-to-

1  
2  
3  
4  
5  
6  
7  
8  
9  
10  
11  
12  
13  
14  
15  
16  
17  
18  
19  
20  
21  
22  
23  
24  
25  
26  
27  
28  
29  
30  
31  
32  
33  
34  
35  
36  
37  
38  
39  
40  
41  
42  
43  
44  
45  
46  
47  
48  
49  
50  
51  
52  
53  
54  
55  
56  
57  
58  
59  
60  
61  
62  
63  
64  
65

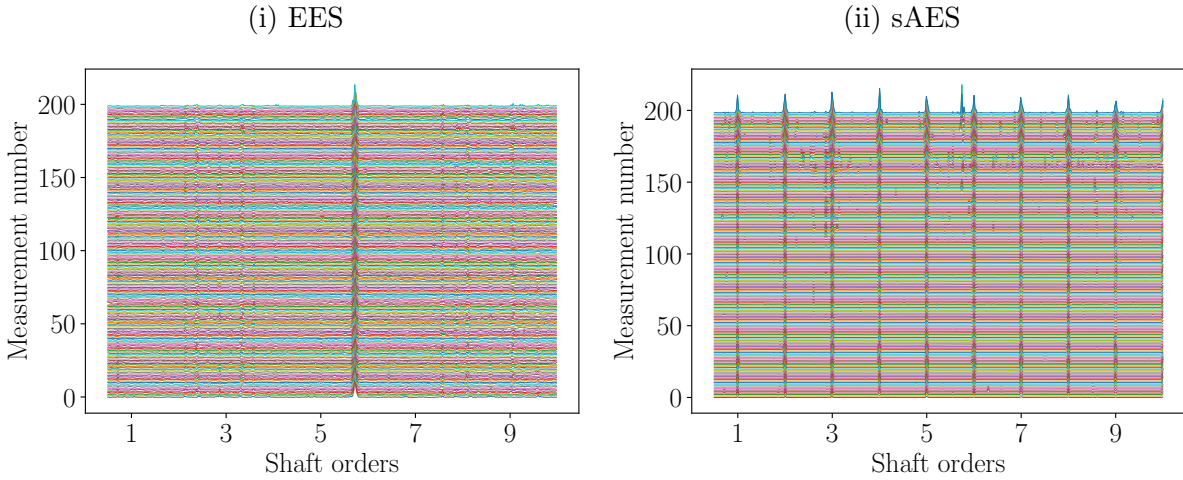


Figure 11: The Enhanced Envelope Spectra (EES) and the smoothed Anomalous Envelope Spectrum (sAES) of the data acquired from the gearbox with localised gear damage.

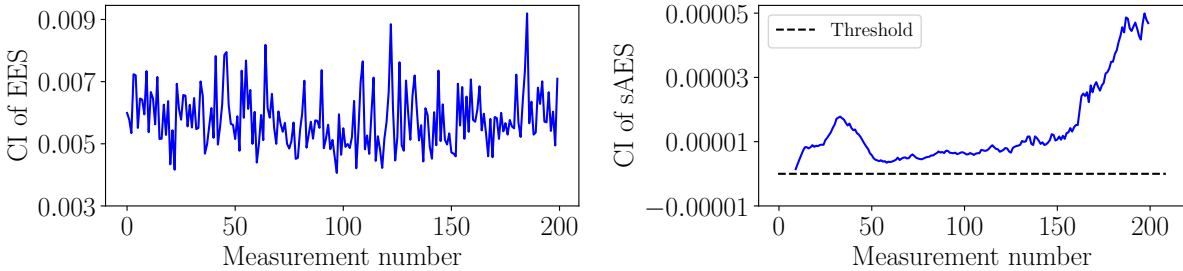


Figure 12: The blind condition indicators of the EES and the sAES are presented over measurement number.

noise ratios of the damaged components are too low in the EES. This is in contrast to the sAES. The CI associated with the sAES is always larger than zero, which indicates that the system contains anomalous information. Initially the CI makes a hump between the first and the 50th measurements, whereafter the CI steadily increases until the gear failed. We do not know the reason behind the hump in the CI at the start of the experiment, since the gearbox was not opened nor inspected between the start of the measurement and the end of the experiment. However, we speculate that this was due to propagation of the gear damage starting in the initial measurements, whereafter it stabilised until the crack reached its critical length.

Comparing the results against the results obtained with the raw signal in Appendix C, it is evident that the proposed method highlights the fault information in the vibration

1  
2  
3 signal and makes it possible to see the degrading gear component.  
4  
5

#### 6 *4.3. Distributed gear damage experiment* 7

8  
9 Distributed gear damage modes such as pitting are very frequently encountered in crit-  
10 ical rotating machines such as wind turbine gearboxes [26]. The distributed gear damage  
11 can result in localised gear damage to develop, which could lead to the failure of the gear-  
12 box. Hence, distributed gear damage is also very important to detect, especially under  
13 time-varying operating conditions.  
14  
15  
16  
17  
18

19 The gear of the monitored gearbox was replaced with a healthy gear and tested again.  
20 In the healthy and the testing dataset all operating conditions in Figure 7 are considered.  
21 Forty measurements were again taken from the healthy gearbox whereafter the gearbox  
22 was disassembled and replaced with a different gear that was left in a corrosive environment  
23 for a long time. This gear is presented in Figure 13(a), where the surface damage is clearly  
24 seen. The damaged gear was tested for approximately eight days before the experiment  
25 was stopped due to excessive vibrations that were measured on the gearbox. This damaged  
26 gear after the completion of the experiment is presented in Figure 13(b). After inspecting  
27 the data, it was observed that the gear experienced a tooth failure at approximately the  
28 100th measurement of the 200 considered in this work, which resulted in the higher loads  
29 and impacts on the adjacent teeth. This subsequently resulted in the adjacent gear teeth  
30 to fail in the final stages of the test.  
31  
32  
33  
34  
35  
36  
37  
38  
39  
40  
41  
42  
43

44 The methodology is again similarly applied as in the previous section, where a threshold  
45  $\tau(\alpha, f)$  is obtained of the healthy data, which is subsequently used to calculate the AES  
46 and the sAES. The 200 measurements that were acquired over the life of the gear are  
47 presented in Figure 14 for the EES and the sAES. Both the EES and the SAES are able to  
48 detect the gear damage components at 1.0 shaft orders and its harmonics, but the sAES  
49 contains much lower noise levels. The benefit of the lower noise levels is highlighted when  
50 investigating the condition indicator of the EES and the sAES.  
51  
52  
53  
54  
55  
56  
57  
58

59 The condition indicators of the EES in Figure 15 contains much noise and it is difficult  
60  
61  
62  
63  
64  
65

(a) Before the experiment started

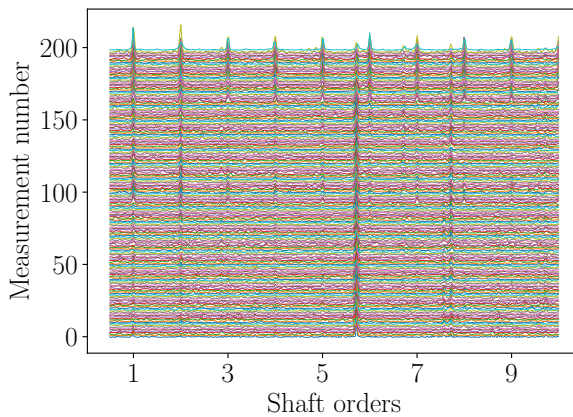


(b) After the experiment was completed



Figure 13: The gear before the experiment started and after the experiment was completed are presented in Figures 13(a) and 13(b) respectively. The damaged regions of the gear are clearly highlighted in Figure 13(b).

(i) EES



(ii) sAES

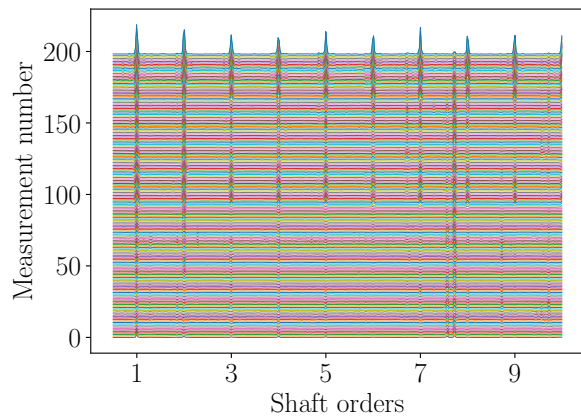


Figure 14: The Enhanced Envelope Spectra (EES) and the smoothed Anomalous Envelope Spectrum (sAES) of the vibration data acquired during the distributed gear damage experiment.

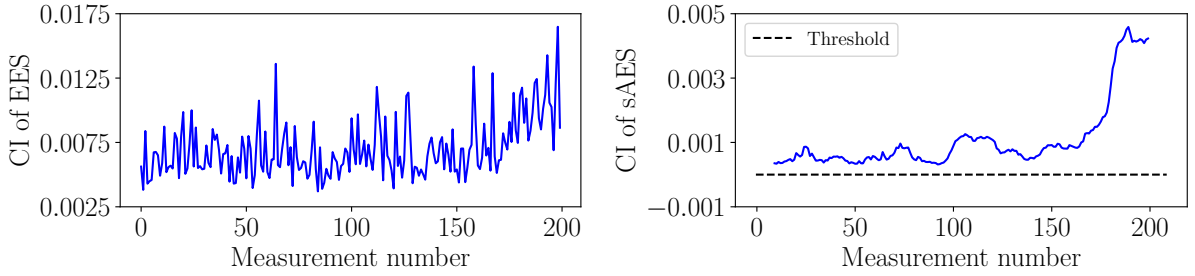


Figure 15: The blind condition indicators calculated with the EES and the sAES are presented over measurement number for the distributed gear damage experiment.

to detect the deterioration of the gear over time. This is in contrast to the results obtained with the sAES condition indicator that is presented in Figure 15. The CI of the sAES is clearly larger than the threshold, which is indicative that the gearbox contains anomalous behaviour. The changes of the CI of the sAES over time, indicates the degradation of the gear, with the two events associated with the failure of the gear teeth seen at approximately the 100th measurement number and the 175th measurement respectively. Hence, the proposed method results in a significant improvement.

The sAES is therefore very capable of not only detecting that there is damage present in the system, but it is also possible to determine the cyclic orders of the anomalous component that is changing over time.

#### 4.4. Healthy gearbox

Vibration data from a healthy gearbox are investigated in this section. This vibration data were not used for estimating the threshold  $\tau(\alpha, f)$ , i.e. we did not use the training data. The integrated spectra (i.e. EES, AES and sAES) are presented for two measurements of the healthy gearbox in Figure 16. The EES is dominated by the 5.72 shaft orders component. The AES contains spurious anomalous components at different cyclic orders, however, these components are random and are removed in the smoothing process as shown in the sAES. The spurious components are attributed to the vibration data from the gearbox being random and the OFSCoh being very sensitive to weak components.

The condition indicators associated with the EES and the sAES are also presented in Figure 16. The EES contains some random fluctuations, but does not have an increasing

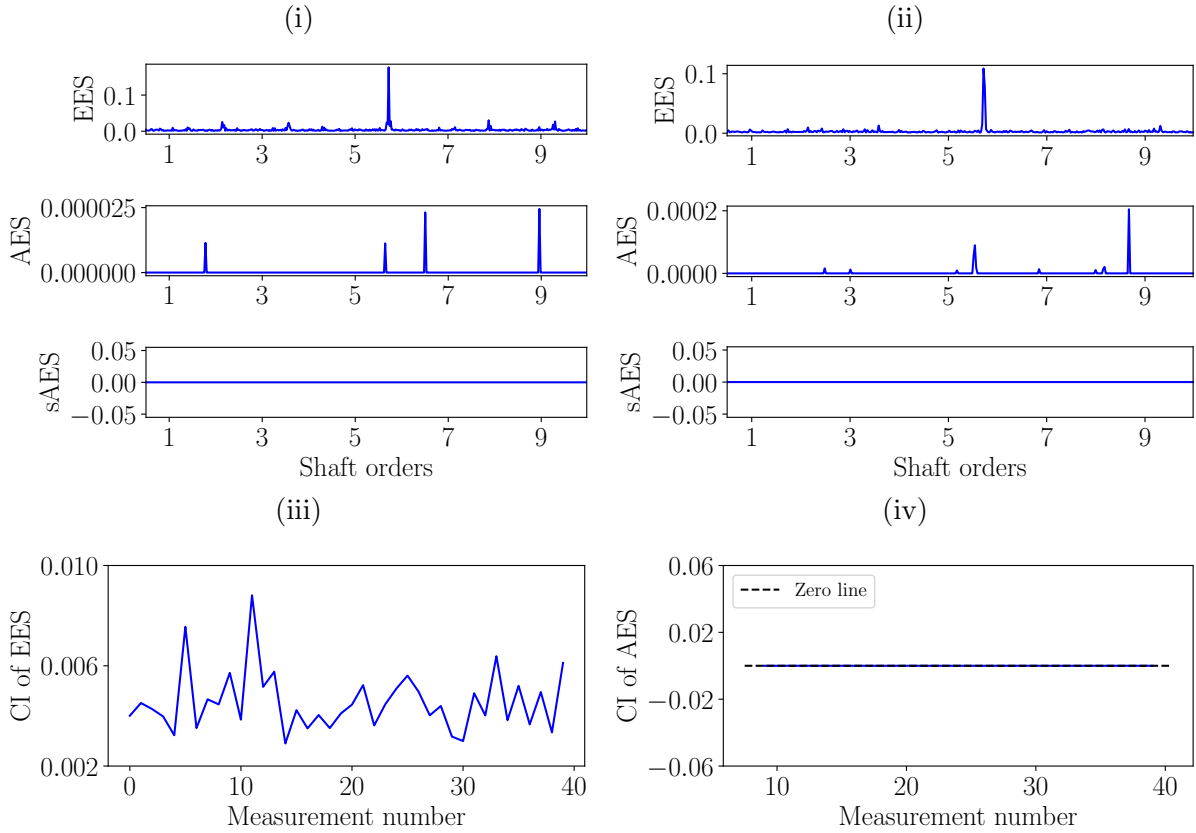


Figure 16: The Enhanced Envelope Spectra (EES) and the smoothed Anomalous Envelope Spectrum (sAES) and their corresponding condition indicators are presented for the vibration data acquired from a healthy gearbox. The healthy gearbox data were acquired from a different experiment compared to the data used in the training procedure.

trend. In contrast the sAES is 0 for all measurements. This is attributed to the removal of the dominant healthy components by the AES, whereafter the smoothing operation removes the spurious noise components. The results therefore indicate that the proposed method allows us to distinguish between a healthy gearbox and a damaged gearbox.

## 5. Additional considerations of the proposed method

Two important aspects of the proposed method are considered in this section, namely,

- the average time required to calculate the AES and sAES; and
- the amount of historical data required to estimate a suitable threshold.

1  
2  
3 *5.1. Average calculation time*  
4

5 The average time to perform the different steps of the proposed method is summarised  
6 in Table 1 for the numerical and the experimental gearbox datasets. The bottleneck in the  
7 proposed method is caused by the calculation of the OFSCoh, which is attributed to the  
8 Welch-based estimator being used to estimate the OFSCoh. As mentioned in Section 2.1,  
9 there are much faster estimators available to calculate the spectral coherence (e.g. [11, 20])  
10 and should be used to reduce the time needed to calculate the AES and the sAES. The  
11

12  
13  
14  
15  
16  
17  
18 **Table 1:** The average time in seconds to perform the different steps is included. This was performed with  
19 a personal computer with 32 Gb of RAM and an AMD Ryzen 7 2700x eight-core processor. Python 3.7.3  
20 was used with NumPy 1.16.4 and SciPy 1.3.0.  
21

Description	Numerical	Experimental
OFSCoh	1193.0918 [s]	325.72 [s]
Weighted OFSCoh	1.22617 [s]	0.2655 [s]
AES and sAES	0.10213 [s]	0.02330 [s]

22  
23  
24  
25  
26  
27  
28  
29  
30 numerical gearbox dataset took longer to calculate because the OFSCoh matrix was larger  
31 than the experimental dataset. This is attributed to the higher rotational speeds, which  
32 required a finer cyclic order resolution; and the OFSCoh of the numerical dataset had  
33 to include higher cyclic orders due to the higher characteristic orders of the components  
34 of interest. The EES, IES, and the IESFOgram [23] would also be calculated from the  
35 estimated OFSCoh and therefore the calculation time is expected to be the same order of  
36 magnitude.  
37  
38  
39  
40  
41  
42  
43  
44

45 *5.2. Influence of the historical data*  
46

47 The proposed method is a novelty enhancement method and has two important aspects  
48 that need to be considered:  
49

- 50 • The quality of the historical data for calculating the threshold.
- 51 • The amount of historical data that is necessary to calculate the threshold.

52  
53  
54  
55  
56  
57  
58 This method relies on the threshold for identifying anomalous components in the order-  
59 frequency spectral coherence. Similarly to novelty detection and semi-supervised learning  
60  
61  
62



1  
2  
3 methods, this threshold is estimated with the available historical data and therefore the  
4  
5 quality of the historical data (e.g. amount of historical data, representation of the healthy  
6  
7 system, presence of outliers) would influence the detection of anomalous components.  
8  
9 Hence, the quality of the historical data would directly influence the performance of the  
10  
11 method, e.g. the method could be either too sensitive to extraneous components and  
12  
13 result in many false positives or be insensitive to damage and therefore result in the  
14  
15 damage to be detected too late. Therefore, we recommend that a large number of healthy  
16  
17 data files are measured to ensure a good estimate of the threshold is obtained. After the  
18  
19 measurements are acquired from the healthy system, it is recommended that the threshold  
20  
21 is estimated and used to monitor the system. This would ensure that the threshold is a  
22  
23 good representation of the healthy system and would allow changes from the healthy  
24  
25 system to be detected.  
26  
27

28  
29 The influence of the number of healthy files on the resulting condition indicator is  
30  
31 shown in Figure 17 for the simulated data. In each sub-figure, a constant number of  
32  
33 healthy files are used, with 10 batches randomly sampled for the 20 and 30 file cases. This  
34  
35 allows us to showcase the variation in the performance of the method. The variation is not  
36  
37 significant between different batches of healthy measurements, since the simulated data  
38  
39 are very well-behaved, i.e. the generative distribution of the healthy data is the similar  
40  
41 between healthy measurements. This is in contrast to experimental measurements that  
42  
43 could contain additional variations due to environmental changes (e.g. temperature) for  
44  
45 example.  
46

47  
48 The same investigation is performed for the experimental dataset where localised dam-  
49  
50 age was introduced in the tooth of the gear of the system. The results are presented in  
51  
52 Figure 18, with the influence of the number of files being much more prominent. For  
53  
54 example, if 20 files are used to obtain the threshold, a significant variation is observed.  
55  
56 This is attributed to the fact that the number of files is small and that variations between  
57  
58 measurements (e.g. changes in environmental temperatures) could have affected the re-  
59  
60 sults. Hence, it is concluded that 20 measurements are insufficient and more measurements  
61  
62  
63  
64  
65



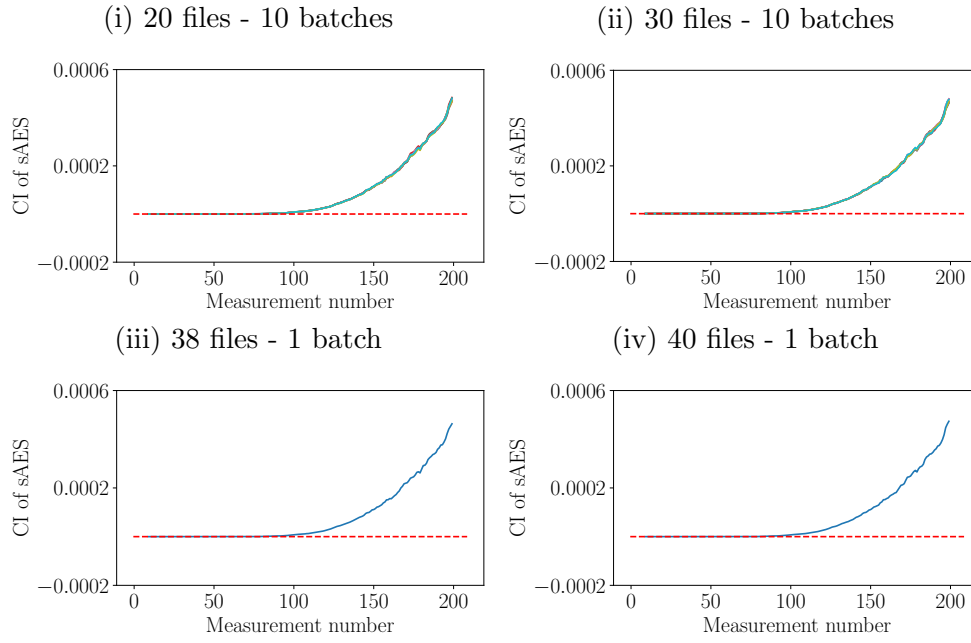


Figure 17: The influence of the number of training files on the condition indicator. Multiple lines on the same plot indicates cases where different batches of the healthy dataset were used.

should be used to reduce the variance of the estimators.

## 6. Conclusions and recommendations

A new methodology is proposed in this work to perform fault diagnosis under time-varying operating conditions. This methodology does not require much knowledge about the kinematics of the machine (i.e. it is blind) nor much human effort to interrogate the results. In this methodology, the order-frequency spectral coherence and healthy historical data are used to calculate an anomalous envelope spectrum, a smoothed anomalous envelope spectrum and a condition indicator. These representations can be used for not only detecting damage in the rotating machine, but it can also be used to identify the damaged components and be used to perform fault trending. The methodology is investigated on a numerical gearbox dataset and three experimental datasets, where it is shown that the proposed method has much potential for performing condition monitoring under time-varying operating conditions.

Future work would investigate and compare different methods of modelling the healthy spectral coherences under time-varying operating conditions (e.g. different threshold se-

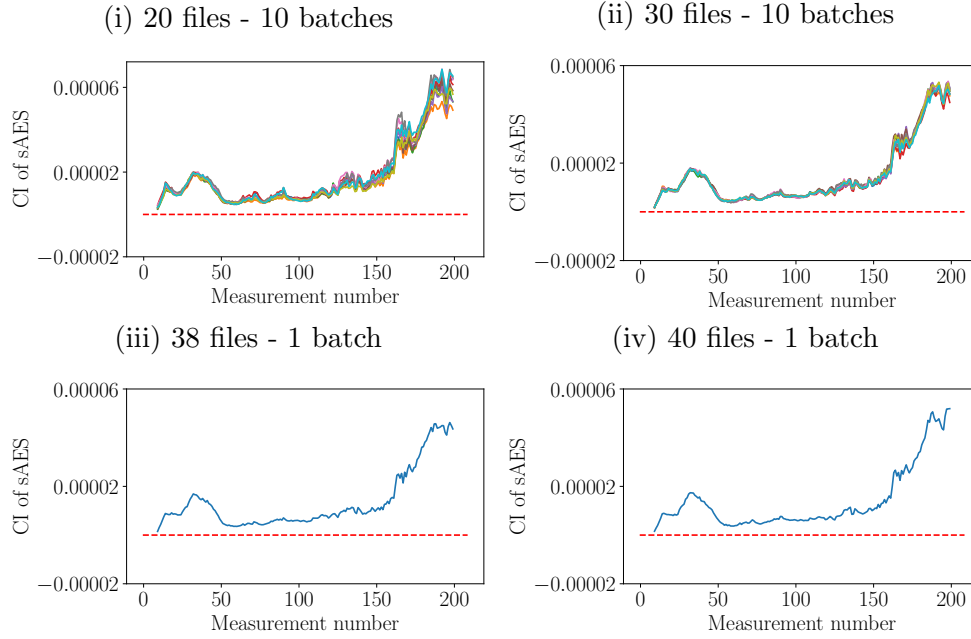


Figure 18: The influence of the number of training files on the condition indicator of the localised gear damage experiment. Multiple lines on the same plot indicates cases where different batches of the healthy dataset were used.

lection procedures); different blind condition indicators that can be extracted from the anomalous envelope spectrum; and also recalibration procedures of the threshold if the gearbox was assembled and disassembled during the monitoring period. **Since the calculation time of the proposed method is governed by the calculation of the order-frequency spectral coherence, the performance of the method using faster estimators will be considered in future work.**

## Appendix A. Threshold selection motivation

If the  $\xi$ th percentile is used in Equation (10) with  $\kappa = 1$  there would be  $100 - \xi\%$  false positives during monitoring. This would therefore result in regular false alarms and should be avoided. The number of false positives can be reduced by selecting  $\kappa > 1$ . In general, care should be taken when selecting  $\kappa > 1$  as this result in extrapolation. However, this is sensible for this application, because of the following reasons:

- The OFSCoh is very sensitive to weak components and therefore large changes are expected in the OFSCoh if damage is present, i.e. it would exceed the threshold

even if  $\kappa > 1$ .

- The distribution of the OFSCoh is known to be chi-squared distributed [7, 10].

In Figure A.19(i), the false positive rates are presented as a function of  $\kappa$  for different distributions. The probability distribution of the OFSCoh is expected to be chi-squared distributed with two degrees-of-freedom if the length of the signal is very long [7, 10] and it is not expected to be uniform, Gaussian or Laplacian distributed. If  $\kappa = 4$ , then very few false positives are expected. However, since the OFSCoh is very sensitive to weak damage components, it will still make it possible to detect the damaged components. This is proven by the results in the main document.

Ultimately, the threshold is estimated from a limited number of healthy measurements. This makes the threshold  $\tau$  a random variable with an underlying sampling distribution. In Figure A.19(ii), the results are presented for the case where we use the 5th and 95th percentile of the sampling distribution of  $\tau$  as a threshold. The performance of the method is clearly dependent on the number of measurements that are used to estimate the threshold. However, by using  $\kappa = 4$  on the OFSCoh data, the results are deemed sufficient for this paper.

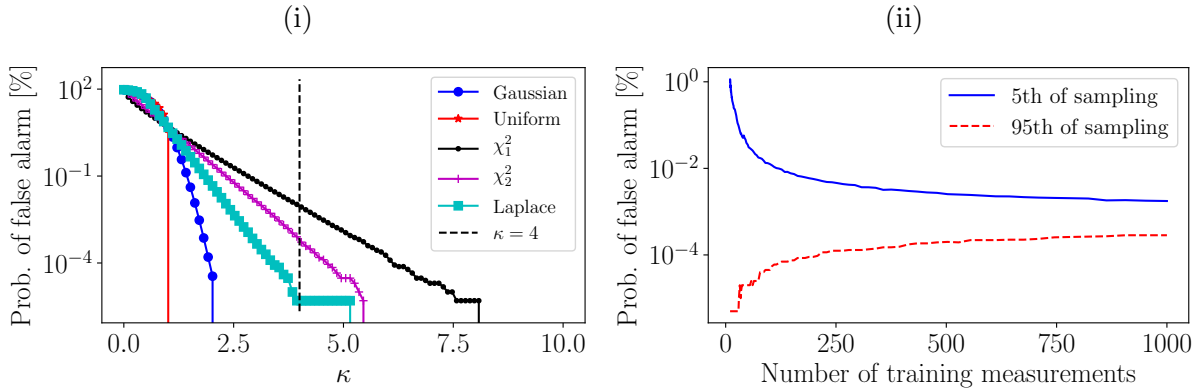


Figure A.19: In Figure A.19(i) the probability of a false alarm is presented for different distributions, calculated using samples from the same distribution as a function of  $\kappa$  in Equation (10). In Figure A.19(ii), the probability of a false alarm is presented for a chi-squared distribution for two degrees of freedom as a function of  $N$  using the 5th and 95th percentile of the sampling distribution for calculating the threshold. This illustrates the variance in the results that can be expected when using a limited number of samples for estimating the threshold  $\tau$  with  $\kappa = 4$ .

## Appendix B. Phenomenological gearbox model

The model used in this work is based on the model used in Ref. [4]. However, it is important to summarise the signal components for understanding the model. The casing vibration signal of the gearbox with bearing damage can be decomposed as

$$x_c(t) = x_{gmc}(t) + x_{dgd}(t) + x_b(t) + x_n(t), \quad (\text{B.1})$$

The gear mesh component is attributed to the deterministic gear mesh interactions and is calculated with

$$x_{gmc}(t) = M(\omega(t)) \cdot h_{gmc}(t) \otimes \left( \sum_{k=1}^{N_{gmc}} A_{gmc}^{(k)} \cdot \sin \left( k \cdot N_{teeth} \cdot \int_0^t \omega(\tau) d\tau + \varphi_{gmc}^{(k)} \right) \right), \quad (\text{B.2})$$

where  $M(\omega(t)) = \omega^2$  simulates the dependence of the signal-component to rotational speed. The impulse response function  $h_{gmc}(t)$  is approximated with a single degree of freedom system with a natural frequency of 2000 Hz and a damping ratio of 0.05. The amplitude and phase of the  $i$ th gear mesh component are denoted by  $A_{gmc}^{(k)}$  and  $\varphi_{gmc}^{(k)}$  respectively. The instantaneous gear mesh frequency is calculated with  $N_{teeth} \cdot \omega(t)$ , where  $N_{teeth}$  is the number of teeth on the gear.

The random gear component is attributed to distributed gear damage and is calculated with

$$x_{dgd}(t) = M(\omega(t)) \cdot h_{dgd} \otimes \left( \varepsilon_\sigma(t) \cdot \sum_{k=1}^{N_{dgd}} A_{dgd}^{(k)} \cdot \sin \left( k \cdot \int_0^t \omega(\tau) d\tau + \varphi_{dgd}^{(k)} \right) \right), \quad (\text{B.3})$$

which has the same form as the gear mesh component, except for the additional variable  $\varepsilon_\sigma(t)$ . The variable  $\varepsilon_\sigma(t)$  is sampled from a standardised Gaussian and simulates the interactions between the damaged gear teeth during meshing. The single degree-of-freedom impulse response function of the distributed gear damage component  $h_{dgd}(t)$  has a natural frequency of 1300 Hz and a damping ratio of 0.05.

The broadband noise component is calculated with

$$x_n(t) = M(\omega(t)) \cdot \epsilon_\sigma(t) \quad (\text{B.4})$$

which consists of standardised Gaussian noise  $\epsilon_\sigma(t)$  being scaled by changes in rotational speed with  $M(\omega(t))$ .

Bearing damage on the outer race of a rolling element bearing would result in impacts as the rolling elements move in-and-through the defective area. These impacts result in broadband excitation of the structure as it is filtered from the source of the bearing damage through the structure to the transducers. The measured outer race bearing damage signal is simulated with

$$x_b(t) = M(\omega(t)) \cdot h_b(t) \otimes \left( \sum_{k=0}^{N_{imp}-1} A_b^{(k)} \cdot \delta \left( t - T_b^{(k)} \right) \right), \quad (\text{B.5})$$

where the impulse response function of the bearing damage component  $h_b(t)$  has a natural frequency of 7000 Hz and a damping ratio of 0.05. The signal contains  $N_{imp}$  impulses, with the  $k$ th impulse having a time-of-arrival given by  $T_b^{(k)}$  and its magnitude is scaled with  $A_b^{(k)}$ .

Since it is desired to investigate the ability of the proposed method to perform fault trending the magnitude of the bearing damage component is scaled as shown in Figure B.20. The RMS of the resulting bearing signals are also presented over measurement number.

### Appendix C. Experimental results

The root-mean-square of the raw vibration signal; the kurtosis of the raw vibration signal; and the L2/L1 norm ratio of the SES of the raw order tracked signal are presented in Figure C.21. The RMS is very sensitive to time-varying operating conditions and does not clearly indicate that the gear is damaged for the localised gear and distributed gear damage

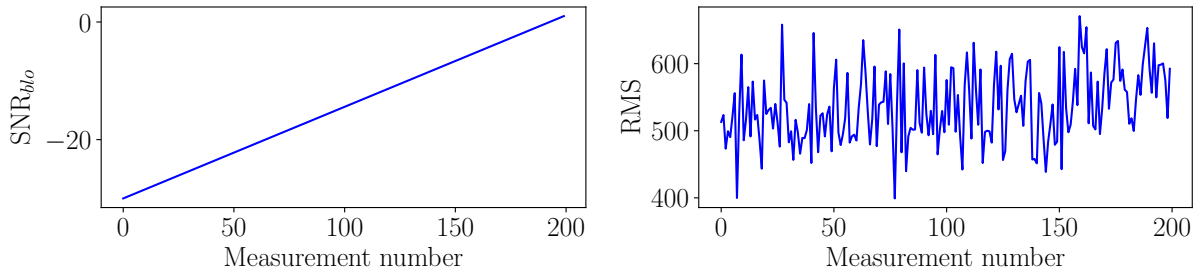


Figure B.20: The signal-to-noise ratio and the Root-Mean-Square (RMS) of the damaged bearing component are presented over measurement number. The signal-to-noise ratio is calculated with  $10 \log_{10}(E_b/E_n)$  where  $E_b$  is the energy of the bearing component and  $E_n$  is the energy of the noise component.

experiment. The kurtosis performs better than the RMS for both cases, but it contains much more noise than the condition indicators obtained with the proposed methodology. The L2/L1 ratio of the SES does not perform well on the considered dataset. Hence, it is clear that the proposed method performs very well in highlighting that the gearbox is damaged and that its health is deteriorating over measurement number.

## Acknowledgements

S. Schmidt gratefully acknowledges the Eskom Power Plant Engineering Institute (EPPEI) for their support in the execution of this research.

## References

- [1] J. Antoni, Cyclostationarity by examples, *Mechanical Systems and Signal Processing* 23 (4) (2009) 987–1036.
- [2] V. Girondin, K. M. Pekpe, H. Morel, J.-P. Cassar, Bearings fault detection in helicopters using frequency readjustment and cyclostationary analysis, *Mechanical Systems and Signal Processing* 38 (2) (2013) 499–514.
- [3] R. B. Randall, J. Antoni, S. Chobsaard, The relationship between spectral correlation and envelope analysis in the diagnostics of bearing faults and other cyclostationary machine signals, *Mechanical Systems and Signal Processing* 15 (5) (2001) 945–962.

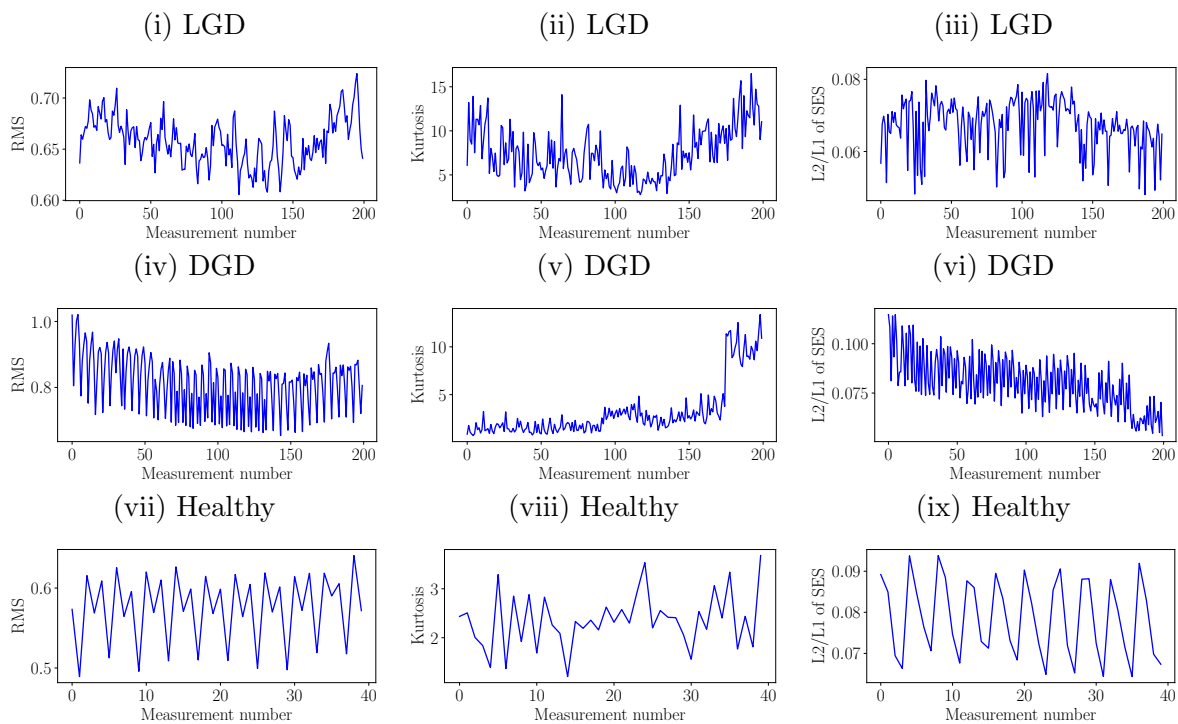


Figure C.21: Three blind metrics are calculated for different experimental signals considered in this work. Abbreviations: Localised Gear Damage (LGD) discussed in Section 4.2; Distributed Gear Damage (DGD) discussed in Section 4.3.

- [4] D. Abboud, J. Antoni, S. Sieg-Zieba, M. Eltabach, Envelope analysis of rotating machine vibrations in variable speed conditions: A comprehensive treatment, *Mechanical Systems and Signal Processing* 84 (2017) 200–226.
- [5] J. Urbanek, T. Barszcz, R. Zimroz, J. Antoni, Application of averaged instantaneous power spectrum for diagnostics of machinery operating under non-stationary operational conditions, *Measurement* 45 (7) (2012) 1782–1791.
- [6] N. Baydar, A. Ball, Detection of gear deterioration under varying load conditions by using the instantaneous power spectrum, *Mechanical Systems and Signal Processing* 14 (6) (2000) 907–921.
- [7] J. Antoni, Cyclic spectral analysis in practice, *Mechanical Systems and Signal Processing* 21 (2007) 597–630.

- 1  
2  
3 [8] J. Antoni, Cyclic spectral analysis of rolling-element bearing signals: Facts and fic-  
4 tions, *Journal of Sound and Vibration* 304 (3-5) (2007) 497–529.  
5  
6  
7  
8 [9] R. Zimroz, W. Bartelmus, T. Barszcz, J. Urbanek, Diagnostics of bearings in pres-  
9 ence of strong operating conditions non-stationarity - A procedure of load-dependent  
10 features processing with application to wind turbine bearings, *Mechanical Systems*  
11 *and Signal Processing* 46 (1) (2014) 16–27.  
12  
13  
14  
15  
16  
17 [10] D. Abboud, S. Baudin, J. Antoni, D. Rémond, M. Eltabach, O. Sauvage, The spectral  
18 analysis of cyclo-non-stationary signals, *Mechanical Systems and Signal Processing*  
19 75 (2016) 280–300.  
20  
21  
22  
23  
24 [11] J. Antoni, G. Xin, N. Hamzaoui, Fast computation of the spectral correlation, *Me-*  
25 *chanical Systems and Signal Processing* 92 (2017) 248–277.  
26  
27  
28  
29 [12] A. Mauricio, J. Qi, W. A. Smith, M. Sarazin, R. B. Randall, K. Janssens, K. Gryllias,  
30 Bearing diagnostics under strong electromagnetic interference based on integrated  
31 spectral coherence, *Mechanical Systems and Signal Processing* 140 (2020) 106673.  
32  
33  
34  
35  
36 [13] D. Wang, X. Zhao, L.-L. Kou, Y. Qin, Y. Zhao, K.-L. Tsui, A simple and fast guideline  
37 for generating enhanced/squared envelope spectra from spectral coherence for bearing  
38 fault diagnosis, *Mechanical Systems and Signal Processing* 122 (2019) 754–768.  
39  
40  
41  
42 [14] S. Schmidt, P. S. Heyns, K. C. Gryllias, A methodology using the spectral coherence  
43 and healthy historical data to perform gearbox fault diagnosis under varying operating  
44 conditions, *Applied Acoustics* 158 (2020) 107038.  
45  
46  
47  
48  
49  
50 [15] F. Jia, Y. Lei, J. Lin, X. Zhou, N. Lu, Deep neural networks: A promising tool  
51 for fault characteristic mining and intelligent diagnosis of rotating machinery with  
52 massive data, *Mechanical Systems and Signal Processing* 72-73 (2016) 303–315.  
53  
54  
55  
56  
57  
58 [16] Z. Chen, A. Mauricio, W. Li, K. Gryllias, A deep learning method for bearing fault  
59  
60  
61  
62  
63  
64  
65



- 1  
2  
3 diagnosis based on cyclic spectral coherence and convolutional neural networks, *Mechanical Systems and Signal Processing* 140 (2020) 106683.  
4  
5  
6  
7  
8 [17] S. Schmidt, P. S. Heyns, An open set recognition methodology utilising discrepancy  
9 analysis for gear diagnostics under varying operating conditions, *Mechanical Systems  
10 and Signal Processing* 119 (2019) 1–22.  
11  
12  
13  
14 [18] Q. Leclère, H. André, J. Antoni, A multi-order probabilistic approach for Instanta-  
15 neous Angular Speed tracking debriefing of the CMMNO'14 diagnosis contest, *Mechanical Systems and Signal Processing* 81 (2016) 375–386.  
16  
17  
18  
19  
20 [19] S. Lu, R. Yan, Y. Liu, Q. Wang, Tacholless speed estimation in order tracking: A  
21 review with application to rotating machine fault diagnosis, *IEEE Transactions on  
22 Instrumentation and Measurement* 68 (7) (2019) 2315–2332.  
23  
24  
25  
26  
27 [20] P. Borghesani, J. Antoni, A faster algorithm for the calculation of the fast spectral  
28 correlation, *Mechanical Systems and Signal Processing* 111 (2018) 113–118.  
29  
30  
31  
32  
33 [21] R. B. Randall, J. Antoni, Rolling element bearing diagnosticsa tutorial, *Mechanical  
34 systems and signal processing* 25 (2) (2011) 485–520.  
35  
36  
37  
38  
39 [22] W. A. Smith, P. Borghesani, Q. Ni, K. Wang, Z. Peng, Optimal demodulation-band  
40 selection for envelope-based diagnostics: A comparative study of traditional and novel  
41 tools, *Mechanical Systems and Signal Processing* 134 (2019) 106303.  
42  
43  
44  
45  
46 [23] A. Mauricio, W. A. Smith, R. B. Randall, J. Antoni, K. Gryllias, Improved envelope  
47 spectrum via feature optimisation-gram (iesfogram): A novel tool for rolling element  
48 bearing diagnostics under non-stationary operating conditions, *Mechanical Systems  
49 and Signal Processing* 144 (2020) 106891.  
50  
51  
52  
53  
54 [24] D. Wang, Spectral l2/l1 norm: A new perspective for spectral kurtosis for character-  
55 izing non-stationary signals, *Mechanical Systems and Signal Processing* 104 (2018)  
56 290–293.  
57  
58  
59  
60  
61  
62  
63  
64  
65

1  
2  
3  
4  
5  
6  
7  
8  
9  
10  
11  
12  
13  
14  
15  
16  
17  
18  
19  
20  
21  
22  
23  
24  
25  
26  
27  
28  
29  
30  
31  
32  
33  
34  
35  
36  
37  
38  
39  
40  
41  
42  
43  
44  
45  
46  
47  
48  
49  
50  
51  
52  
53  
54  
55  
56  
57  
58  
59  
60  
61  
62  
63  
64  
65

[25] J. Antoni, The infogram: Entropic evidence of the signature of repetitive transients, *Mechanical Systems and Signal Processing* 74 (2016) 73–94.

[26] Y. Lin, L. Tu, H. Liu, W. Li, Fault analysis of wind turbines in China, *Renewable and Sustainable Energy Reviews* 55 (2016) 482–490.